TAMPEREEN TEKNILLINEN YLIOPISTO
TAMPERE UNIVERSITY OF TECHNOLOGY

AIDA KHAYYAMI
LOW TEMPERATURE SOL-GEL ON POLYMERIC SUBSTRATE
Master of Science Thesis

ABSTRACT

Due to the flexibility in preparation process, the sol-gel method has gained a huge interest from the industry and also various studies have been conducted in this area. The processing temperatures are low and there is a wide possibility to vary different synthesis parameters to achieve coatings with optimized properties. The process begins from a solution in which, particles and clusters are produced by hydrolysis and condensation reactions, results in to the formation of a sol. The particles and clusters will grow and aggregate and form a gel, which will be dried and heat treated. In this study, sol-gel method was used to apply thin films on polymeric biosensors to protect the conductive layers from reacting with water. This may lead to improve the durability and stability of the resonance characteristics of biosensors in aqueous environment.

Two types of inorganic and hybrid sol-gels were prepared in this study. The inorganic TiO_2 films were densified using a laser, in order to heat the film locally and prevent the destruction of polymeric substrate. In the second step, a hybrid sol-gel (organic/inorganic) was developed, to allow curing using heat treatment at temperature adequate to maintain the structural integrity of the substrate. The hybrid sols were prepared by hydrolysis and condensation of γ-methacryloxypropyltrimethoxysilane 98% (MAPTMS) and titanium butoxide at different molar ratios, aging time, curing temperature and number of layers.

Structural characterization of the coatings was performed using scanning electron microscopy (SEM), fourier transform infrared (FTIR) spectroscopy, atomic force microscopy (AFM), and optical microscopy. Contact angle measurement was performed to investigate the hydrophilicity of the coatings. Immersion experiments were conducted in simulated body fluid (SBF) to evaluate the corrosion resistance of the coatings.

The results indicate that, the lasers that are working in the UV and IR spectral region should be used for densification of titania films. On the other hand, it was found that, corrosion resistance of hybrid coatings was influenced by the molar ratios of MAPTMS: titanium butoxide and number of layers of applied film. It was seen that, coatings at higher inorganic content had higher porosity and as a result, lower corrosion resistance. A higher corrosion resistance behavior for samples with five layers also was noticed.

It was concluded that, the most promising samples were the ones containing lower inorganic content which were cured at 60˚C and containing five layers.

PREFACE

This thesis has been written to fulfil the requirements of Master of Science degree in Biomedical Engineering. The thesis work has been carried out in the Department of Electronics and Communications Engineering at Tampere University of Technology.

First of all, I would like to express my gratitude and sincere thanks to my supervisors, Professor Dr Tech Minna Kellomäki and Academy Research Fellow Jonathan Masserafor their patient, guidance and helpful advices. This thesis would not have been completed without their help and support.

I would like to thank all my colleagues at the university especially the Biomaterial and Tissue Engineering group I owe my deepest gratitude for the pleasant work atmosphere.

I want to thank all my dear friends and family who continue to enrich my life beyond measure. I am deeply grateful to my sister Shabnam for her support with not only my work but with all other aspects of life. Moreover; I would like to express my appreciation to Mohammad Mehdi for his support and encouragement through all the time I was doing my thesis. Last and definitely not least I wish to give my heartfelt thanks to my parents, Bahman and Masi, for all their love, kindness and motivations through my life. Thank you for always being there for me and for encouraging me to be the best I can be.

Aida Khayyami
Tampere, May 2015

Contents

ABBREVIATIONS

AFM	Atomic force microscopy
APTES	3-aminopropyltriethoxysilane
APTMS	3-aminopropyltrimethoxysilane
ATR	Attenuated total reflectance
BSE	Back scattered electrons
CERAMERS	Ceramic polymers
CO_2	Carbon dioxide
CVD	Chemical vapor deposition
EDX	Energy dispersive X-ray
EPD	Electrophoretic deposition
FSP	Flame spray pyrolysis
FTIR	Fourier transform infra-red
GPMEOS	3-glycidoxypropyltrimethoxysilane
GPTS	3-glycidyloxypropyl trimethoxysilane
IR	Infrared
MAPTMS	γ-methacryloxypropyltrimethoxysilane
Mg	Magnesium
MPS	3-methacryloxypropyltrimethoxysilane
Nd: YAG	Neodymium-doped yttrium aluminium garnet
Ormocers	Organically modified ceramics
ORMOSILS	Organically modified silicates
PLA	Poly (lactic acid)
PLD	Pulsed laser deposition
POLYCERAM	Polymeric ceramic
PVD	Physical vapor deposition
PZC	Point of zero charge
SBF	Simulated body fluid
SE	Secondary electrons
SEM	Scanning electron microscopy
SGLIT	Sol-gel/laser-induced technique
SiO_2	Silicon dioxide
T_g	Glass transition temperature
TiO_2	Titanium dioxide
T_m	Melting temperature
TMOS	Tetramethoxy silane
TMSph	Tris (trimethylsilyl) Phosphate
T_x	Crystallization temperature
UV	Ultraviolet
ZrTPO	Zirconium (IV) propoxide

1 INTRODUCTION

1.1 Research motivation

Passive LC resonant sensors have attracted much interest to measure pressure, temperature or even humidity in a wireless manner and in harsh environment [1]. Such sensors can also found great applications in the biomedical field as implantable sensors. Implantable sensors, to be placed into the body of a patient, would be a great advantage since the measurement is not prevented by the sensor-skin interface. The biosensors can be implanted at an unavoidable surgical operation due to injury or disease. In the best case, the sensor would be fully biodegradable, i.e. that all parts of the sensors would be assimilated by the body after sufficiently long period of time. A biodegradable sensor brings much interest since a second surgery to remove the implant after its period of use would be avoided, thereby the patient's comfort and safety would be improved considerably [1].

To create a biodegradable resonant circuit, methods to produce biodegradable patterned conductive and isolating layers should be used. Conductive parts or layers made of biodegradable metals (zinc, iron and magnesium), which can be evaporated on biodegradable sheets (biodegradable polymers such as PLA) by using a 3D printed mask [1]. However, the short durability in aqueous environment and the instability of the resonance characteristics was reported as the main drawbacks of such biosensors [1]. Indeed, in the case of Mg, taken as an example, one atom of Mg generates one hydrogen gas molecule [2]. Such readily occurring reaction in aqueous media prevents any practical use of such device.

To solve the problem, one option is to protect the magnesium layer by a coating. Inorganic thin film, pertaining to their good chemical stability, corrosion resistance and bioactivity, can improve both the biocompatibility of the implants and life span of the device upon implantation. Thus coating of sensors with inorganic thin films has attracted much interest. Many methods are available to prepare thin inorganic films: chemical vapor deposition (CVD), electron beam evaporation, ion sputtering and the sol-gel method. In comparison with other films technologies the sol-gel process has certain advantages: low process cost, low temperature of heat treatment, high evenness of the films and wide possibility to vary film properties by changing the composition of the solution [3]. Application of thin films using the sol gel process includes different steps such as sol preparation from hydrolysis and condensation of precursors, deposition of the sol on the substrate, drying and calcination [4]. However, one must be aware that typical inorganic thin films processed via the sol-gel route, necessitate elevated drying

temperature, which are not compatible with polymeric substrate. Furthermore, one must bear in mind that incomplete calcination of inorganic sol-gel thin films can be detrimental to the activity of biomolecules and the viability of whole cell due to reminiscence of alkoxide precursors, organic solvents and alcohol by products [5]. To solve the problem, inorganic sol-gel can be cured using sol-gel/laser-induced technique. In this method, the film will be heated and cured locally using an appropriate laser. This can prevent heating up the polymeric substrate and its destruction.

On the other hand, a hybrid sol-gel can be used as a corrosion resistance layer. Properties such as high transparency (glasslike), low processing temperatures, toughness and elasticity (polymer-like), sufficient thermal stability (silicone-like) and hardness, chemical resistance (inorganic solids) can be achieved by combining the organic and inorganic components. Introduction of organic groups in hybrid films can decrease the curing temperature even up to the room temperature [6].

1.2 Aim of the study

The aim of this study is to define a sol-gel recipe, which can be densified at low temperatures (below the glass transition temperature of PLA) while being biocompatible. The coating should degrade in few hours to few weeks to allow reasonable sensing time, but as long time as possible is preferred.

In this regard, purely inorganic and hybrid (organic/inorganic) sol-gels were studied. Titanium dioxide (TiO_2) was selected as the inorganic sol-gel. Sol-gel/laser-induced technique (SGLIT) was used to prepare TiO_2 thin films on polymeric substrate. On the other hand a combination of MAPTMS and titanium butoxide was used as the hybrid sol-gel.

The ratio between the inorganic (titanium butoxide) and organic (MAPTMS) precursor, stirring time, curing temperature and number of layer deposited were studied in light of the thin films physical (roughness, wettability) and structural properties as well as their corrosion resistance.

The morphology and composition of the prepared films was assessed using scanning electron microscopy (SEM) and atomic force microscopy (AFM). The wettability of the PLA and Mg against the various sols was tested to ensure proper wetting during the thin film deposition. The coated samples were also analysed in terms of their hydrophobicity by measuring the contact angle of distilled water on surface of the specimen.

Structural features and functional groups in cured hybrid coatings were characterized by attenuated total reflectance-fourier transform infrared spectroscopy (ATR-FTIR). Corrosion resistance of the coated substrate was evaluated in physiological conditions through immersion tests in simulated body fluid.

1.3 Outline of thesis

The thesis is organized as follows: Chapter 2 reviews the conventional techniques used to prepare thin films. Chapter 3 provides the state of the art regarding inorganic and hybrid coatings for corrosion resistance. In this section the chemistry behind the sol-gel processing is reviewed. Chapter 4 reviews the reasons behind the material and method choice. Chapter 5 will focus on the materials and methods used in this thesis work. The sol-gel manufacturing steps are detailed and the characterization tools employed are described. Chapter 6 provides the results and discussions of the tests performed during this work. Lastly, Chapter 7 summarises the research results and draws the conclusions from the main findings of each experiment carried out. It also presents an outlook and recommendations for future work in the light of the obtained results.

2 THIN FILM APPLICATION METHODS

The application of thin films in modern technology is widespread. The methods employed for thin-film deposition can be divided into two groups based on the nature of the deposition process viz., physical or chemical [7]. In one hand, the physical methods include physical vapor deposition (PVD) such as pulsed laser deposition and sputtering. In the chemical methods, chemical vapor deposition, sol-gel and flame spray pyrolysis are the favored deposition processes. In the following chapter all the mentioned methods will be reviewed and their advantages and disadvantages will be discussed.

2.1 Physical vapor deposition (PVD)

Physical vapor deposition (PVD) is a method that is widely used for application of thin films. In this method the material that is going to be deposited will be vaporized and condensated on a substrate on to which the film is formed. In this method only physical process, such as high temperature evaporation or sputtering is used [8]. Pulsed laser deposition and sputtering are the most used methods in application of thin films.

2.1.1 Pulsed laser deposition

Figure 2-1 shows the experimental apparatus that is used in pulsed laser deposition (PLD). In this method high-power laser pulses such as an excimer, Nd: YAG or other equivalent laser will be used to evaporate a small amount of matter from a solid target [9].
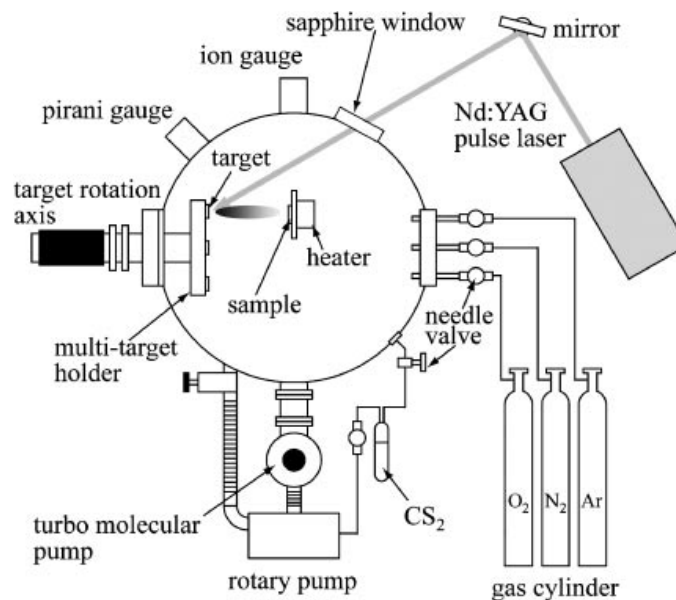
Figure 2-1 Schematic diagram of atmosphere-controlled pulsed laser deposition [10]

The laser beam is focused on the surface of the target. The target surface will absorb the focused laser pulses in a small volume and heat up all the elements rapidly to their evaporation temperature. The high energy of the laser breaks the chemical bond at the surface of the target, producing a high-pressure gas [9].

The produced vapor is a collection of atoms, molecules, ions and electrons. Their amount and kinetic energy is dependent on the laser parameters (intensity, wavelength, pulse width) and the target [11]. According to the laws of gas dynamic the emitted materials moves towards the substrate. Because the dissociated particles have absorbed the laser energy, an expansion of hot plasma (plume) is produced in the deposition chamber. This, in turn, leads to condensation of the particles at the substrate surface forming a thin film after some hundreds or thousands of laser pulses [9]. Different parameters such as spot size of laser, plasma temperature, and target to substrate distance have significant effects on the deposited film uniformity [11].

The laser ablation has several advantages such as maintaining the stoichiometry of the target [12]. The deposited material can be easily changed and a multilayer film can be deposited on the substrate. Placing the laser source outside of reaction chamber makes PLD an easy handling technique in comparison with other methods such as chemical vapor deposition or ion implantation. In addition, growth of adherent and epitaxial films will take place at lower substrate temperature than other methods [11]. However, there are some drawbacks about PLD. Splashing and/or particulates deposition on the film, which will result in an uneven film, required expensive setup, difficulties to achieve a narrow size distribution may limit usage of this method [11, 13, 14].

2.1.2 Sputtering

Sputtering deposition is another PVD technique, which is used to deposit thin films from a target onto a substrate.

In DC sputtering, materials are evaporated from the solid state by bombarding their surfaces with energetic ions; subsequently these ejected atoms will be condensed on the substrate in a high vacuum environment. Figure 2-2, illustrates a sputtering set up.
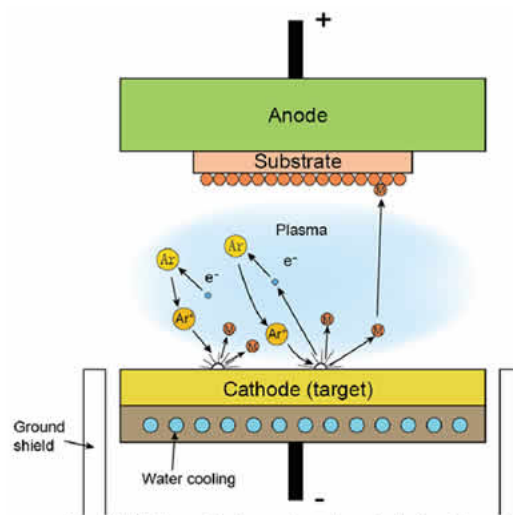

Figure 2-2 DC sputtering [15]

As it can be understood from Figure 2-2, the target is placed at the cathode electrode and the substrate is placed at the anode, which is often at ground potential. A potential is applied across a region near the cathode, and so generates a plasma region (hot gas phase consisting of electrons and ions) near the cathode surface. As the result of collision of these ions on the target surface, atoms will be ejected and will form a film [15].

As it can be understood an electrical conductor material should be used as the cathode since a surface charge will be formed at the surface of the insulating material that will prevent ion bombardment of the target surface [15].

A magnetic field can be added to the DC sputtering system; this magnetic field can deflect the electrons to focus them onto the target surface [15].

An advantage of sputtering is that the plasma is uniformly established over a large area, so that a solid large-area vaporization source can be established. This method has its drawbacks, which limit its application. This method can be used only for simple electrically conductive materials such as metals also the process is rather slow and expensive compared to vacuum deposition [15]. Furthermore, most of the energy incident on the target becomes heat, which limits the application of this method for heat sensitive substrates [16].

2.2 Chemical vapor deposition (CVD)

A popular method for producing high purity, ultra-fine, unagglomerated, strain-free nanocrystalline ceramic powders and also thin nano-composite films is chemical vapor deposition (CVD). In this method, precursor gases flow in a chamber where the heated substrate to be coated stands. The chemical reaction occurs at the vicinity of the substrate surface leading to a thin film deposition [17]. Figure 2-3 shows a schematic diagram of a coating obtained via CVD.
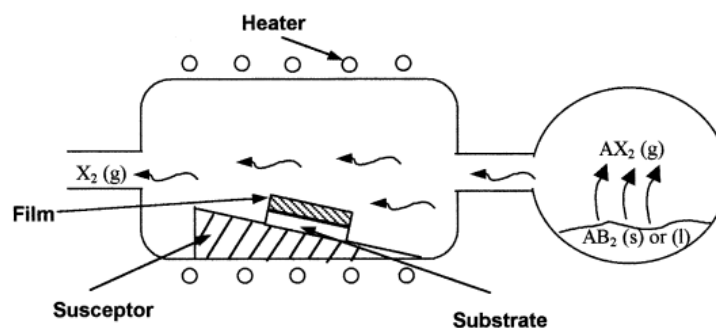
Figure 2-3 A schematic diagram of the CVD coating [18]

There are several significant advantages when using CVD, which make it a preferable process in many cases. Difficult three-dimensional configurations such as deep recesses and holes can usually be coated easily. High rate of deposition and thick coatings makes this process a competitive and, in some cases, more economical than the PVD processes. CVD normally does not require ultrahigh vacuum and generally many pro-

cess variations can be adapted. Furthermore, CVD is highly flexible so that many changes in composition during deposition and the codeposition of elements or compounds can be achieved. CVD also has several disadvantages. The high temperature that is being used in this method limits its use for substrates that are not thermally stable. Another disadvantage of this method is that chemical precursors (the starting materials) with high vapor pressure, which are often hazardous and at times extremely toxic, are required. Furthermore, the by-products of the reactions in CVD are toxic and corrosive and must be neutralized, which may be a costly operation [19].

2.3 Flame spray pyrolysis (FSP)

Ceramic thin films can also be deposited by flame spray pyrolysis (FSP). This method involves spraying a metal salt solution onto a heated substrate. Common spray pyrolysis device consists of different parts such as an atomizer, precursor solution, substrate heater, and temperature controller as seen in Figure 2-4 [7].
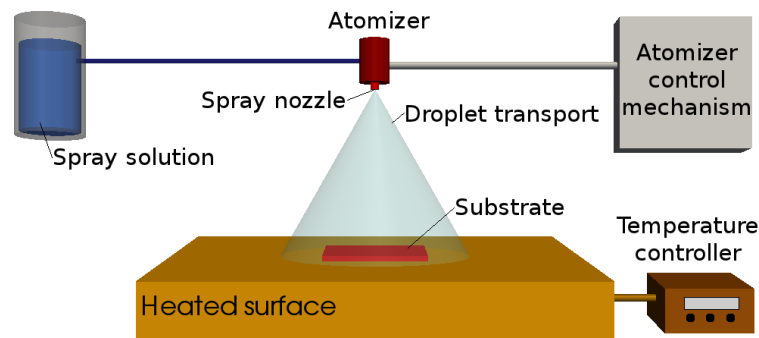

Figure 2-4 General schematic of a spray pyrolysis deposition process [7].

The process entails steps such as atomization of the precursor solution, aerosol transport, and decomposition of the precursor [20]. Air blast, ultrasonic and electrostatic atomizers are normally used in spray pyrolysis techniques. A carrier gas is used to transfer the generated droplets to the flame zone [21].

Due to the high temperature of the flame zone the organometallic precursors decompose and the organic compounds undergo complete combustion. Nucleation and condensation of metallic or semi metallic components of the precursor will result in formation of primary particles [22]. The film would form on the substrate when these particles impact the heated surface and undergo thermal decomposition [20].

A number of advantages are offered by the FSP for processing of ceramic films. The quality and properties of the films are controllable and is dependent on the process parameters such as substrate surface temperature and deposition temperature. Subsequently this method can be used for application of dense or porous films. High quality substrates or chemicals are not required in this method and multi layered films can be easily prepared. Wide range of materials, including simple oxide materials such as SiO_2 and TiO_2 and more complex materials including multicomponent, composites, and non-oxides can be applied as thin films [20].

Porosity is one of the main disadvantages of thermal spray coatings, allowing the passage of gases and/or liquids through the coating/substrate interface. Porosity can be controllable only down to levels below approximately 0.1%. Poor adhesion in comparison to other methods is other limitation of this method [23].

2.4 Sol-gel

A wet-chemical technique that is being widely used in the fields of materials science and ceramic engineering is sol-gel process. In this method, an integrated network (gel) will be formed from a sol of either discrete particles or network polymers [24].

Polymeric sols will be formed from hydrolysis and condensation of metal alkoxides, which are typical precursors. On the other hand particulate sols are made by mechanically mixing of colloidal particles. Gels are formed in polymeric sol-gels as hydrolysis and condensation promotes. In case of particulate sols, a gel will be obtained by reducing the stability of sol.

The liquid phase needs to be removed so that the gel like properties can be achieved. In this regard, a drying process will be used to remove any trace of solvents that may have been trapped during gelation. The drying process is typically accompanied by significant shrinkage and densification of the body. Finally, a thermal treatment, or firing process, is often necessary in order to favor further polycondensation and enhance mechanical properties and structural stability. The firing process induces sintering, densification and grain growth [24].

As it can be illustrated from Figure 2-5 the precursor sol can either be deposited on substrate to form a film (e.g., by dip coating or spin coating), cast into a suitable container with the desired shape (e.g., to obtain monolithic ceramics, glasses, fibers, membranes, aerogels), or used to synthesize powders (e.g., microspheres, nanospheres) [24].
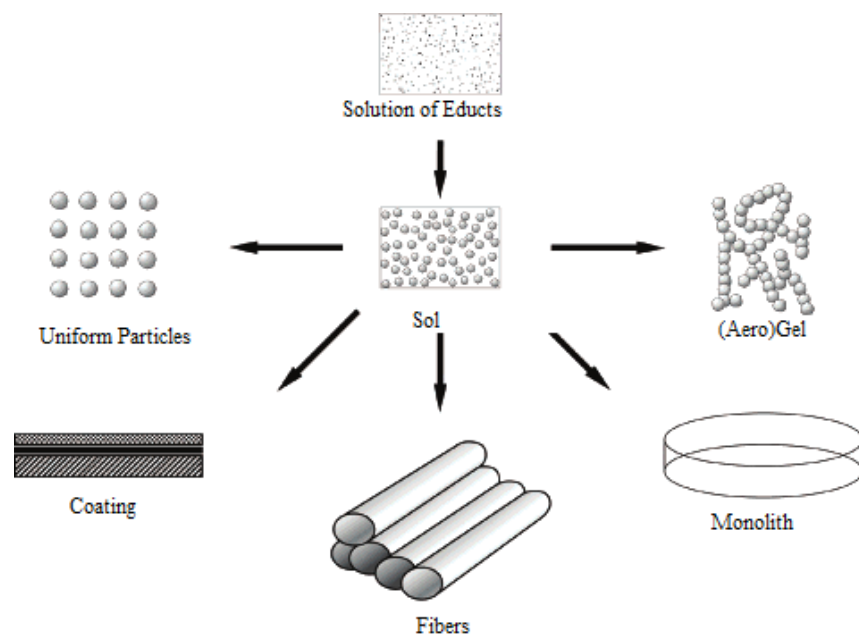

Figure 2-5 Various sol-gel processes

2.5 Conclusion

It can be concluded that CVD and PVD cannot be used in our study due to the high temperature that is required in these methods. Indeed such high temperature is not suitable in case of heat sensitive substrates (polymers). PLD is not a suitable method either since it will result in an uneven deposited film and required expensive setup. The formed porosities in FSP make this method unsuitable in case of corrosion resistance applications since the gases and/or liquids can pass through the coating/substrate interface. On the other hand sol-gel method is the most suitable method for preparation of thin and nanostructured coatings. The main advantages of the processing of the sol-gel derived materials are: low processing temperature, large coated area, low cost, control over purity and composition, easy introduction of dopant and possibility to cast coating in complex shapes. Different simple techniques such as dip coating, spin coating, spraying and electro deposition can be used for application of the sol-gel on a substrate [25].

Protective and functional coatings are the new industrial application areas in which the sol–gel process currently has been focused on. This method allows tailoring the substrate surface properties while preserving those of the bulk. Due to its simplicity, low equipment costs and promising commercial possibilities, this technique competes with surface engineering technologies such as PVD and CVD. Different methods for sol preparation such as (colloidal or hydrolysis–polycondensation), the synthesis parameters (pH, precursors, H_2O/precursor ratio, temperature of reaction, sol concentration, viscosity and density) and the thermal treatment for consolidation and/or sintering can be used in order to achieve wide range of coating compositions and properties. Distinctive characteristics, such as reactivity, hydrophilicity, roughness can be reached by selection of the appropriate coating method and deposition parameters. Moreover, a number of the films properties, such as hardness, critical thickness, wear resistance; chemical behavior, hydrophobicity and adherence can be specified by the sol characteristics and choice of thermal treatments [26]. Figure 2-6 compares different methods that are being used for application of thin film.
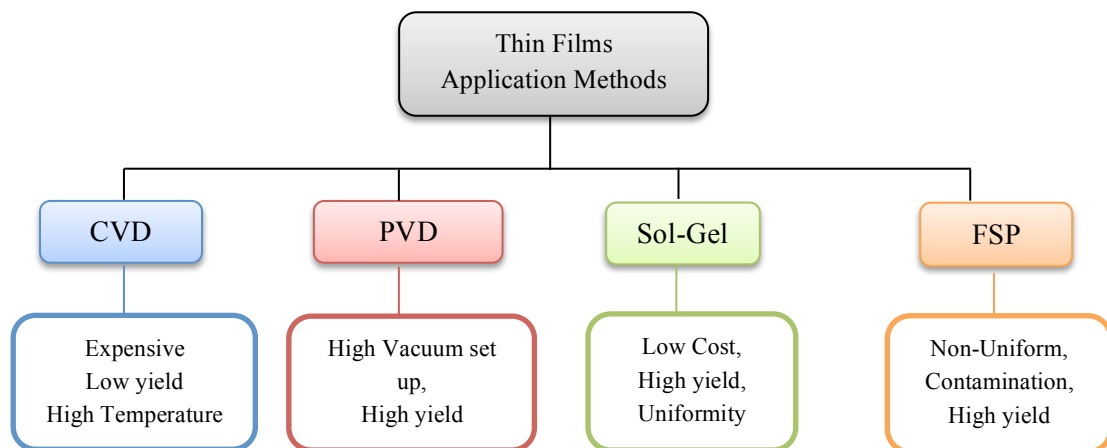

Figure 2-6 Schematic flow chart of various synthesis to prepare thin film

3 TYPES OF SOL-GELS

In the first step of the sol–gel process, a sol will be formed by dissolution of the precursors in a solvent. Sols are stable suspensions of colloidal particles or oligomers (small polymers) within a liquid [27].

There are two different sol-gel routes which are commonly used: (1) the particulate (or colloidal) gel route, in which the sol consist of dense colloidal particles (1 to 1000 nm) and (2) the polymeric gel route, in which the sol consists of polymer chains but has no dense particles >1 nm [27].

Particulate sols are typically formed by mechanical mixing of colloidal particles in aqueous solutions (in which the only liquid present is water) at a pH that prevents precipitation. On the other hand polymeric sols are generally obtained from hydrolysis of alkoxide in nonaqueous solutions containing solvents other than or in addition of water [28, 4].

The particulate and polymeric gels are different in structure and properties. The particulate gels have much larger pores in comparison with polymeric gels. Larger pores cause higher permeability and lower capillary stress during drying which cause less shrinkage and consequently less probability of cracking during drying. On the other hand the average pore size of polymeric gels is much finer than of colloidal gels. Having very fine pores which will cause large capillary stresses during the drying so polymeric gels are prone to cracking. The driving force for sintering is also much higher in polymeric gels resulting in lower sintering temperature. Preparation of thin films is the most important application of the polymeric gels [27].

3.1 Particulate sol-gel

As it was mentioned before, particulate sols are typically formed by mechanical mixing of colloidal particles in aqueous solutions at a pH that prevents precipitation. Due to the growth or agglomeration of primary particles, larger particles with the size in the range of 1-1000 nm will be established in the solvent and form a sol. Due to small size of the dispersed particles, the gravity is negligible and the interactions are dominated by the Van der Waals, electrostatic and steric forces [27].

Attractive Van der Waals forces exist between the particles in the sol and will cause the particles to collide and stick together and lead to rapid sedimentation of particle clusters (i.e., to flocculation or coagulation). A stable sol is obtained when these Vander Waals forces are overcome with repulsive forces and so the flocculation will not occur. There are several ways for achieving this, which includes electrostatic stabilization, steric stabilization and electrostatic stabilization [27].

3.1.1 Stability of sol

In electrostatic stabilization, repulsions are based on the particles electrostatic charges. The particles that are dispersed in the liquid, acquire surface charge in different ways such as preferential adsorption of the ions, dissociation of surface groups, isomorphic substitution or adsorption of charged polymers [27].

Adsorption of the ions is the most common process to stabilize a sol. In this regard, an electrolyte such as an acid, a base or a metal salt will be added to the aqueous liquid. Absorption of these ions on the surface of dispersed particles can cause a charge on the surface [29]. The process will start by hydration of the ceramic particles in an aqueous liquid. Due to hydration of the metal particles, MOH groups will form at their surface. By addition of the acid to the solution, H^+ ions will be adsorbed and the surface of the particle will consequently be charged positively. On the other hand by adding base, OH^- ions will be adsorbed and a negatively charged surface will be produced. In other words, the particle surface charge is pH dependent. The particle will be charged positively at low pH and negatively at high pH. The pH at which the particle is neutrally charged and adsorption of H^+ ions and OH^- ions are balanced is called the point of zero charge (PZC). PZC depends on the acid/base properties of the oxide surface. Acidic oxides such as SiO_2 have a low PZC (pH=2-2.5), whereas more basic oxides such as TiO_2 have high PZC (pH=6) [30].

In order to neutralize the system, a cloud of equal and opposite charge will surround each particle that will be called an electrical double layer. As the distance of the particles decrease the double layers of particles will overlap and cause a repulsive force that tends to oppose further approach. The electrical potential of the cloud decreases exponentially as a function of distance from the surface of particle [27].

In polymeric stabilization, both homopolymers (e.g. polystyrene, polyethylene oxide) and copolymers (e.g. polyvinylpyrrolidone/polystyrere) can be used to stabilize the sol by two different mechanisms: steric stabilization and depletion stabilization. In steric stabilization, uncharged polymer chains, which are adsorbed on to the particle surface, are used to stabilize colloidal particles (Figure 3-1) [31].
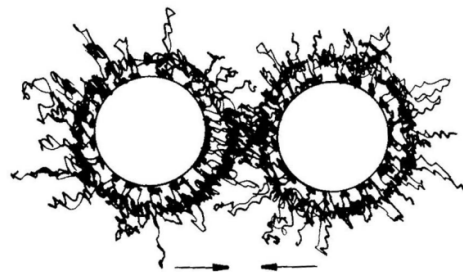

Figure 3-1 Schematics of steric stabilization [31]

On the other hand in depletion stabilization, colloidal particles are imparted by macromolecules that are free in solution (Figure 3-2) [31].
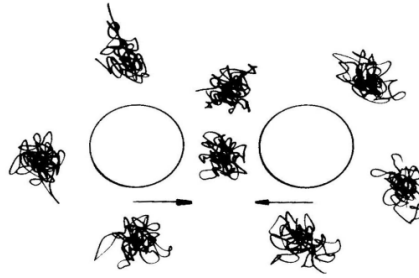
Figure 3-2 Schematics of depletion stabilization [31]

In electrosteric stabilization, the suspension can be stabilized by a combination of electrostatic repulsion and steric repulsion. The origin of the electrostatic component may be a net charge on the particle surface (Figure 3-3 a) and/or charges associated with the polymer attached to the surface (i.e. through an attached polyelectrolyte) (Figure 3-3b) [31].
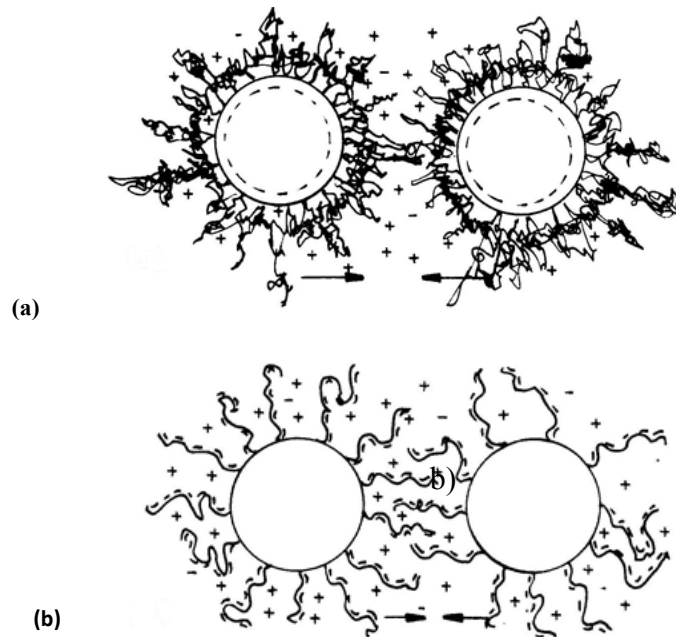

(a)

(b)

Figure 3-3 Schematics of electrosteric stabilization: (a) charged particles with nonionic polyme rs; (b) polyelectrolytes attached to uncharged particles [31].

3.1.2 Gelation

Particulate gels are commonly prepared by taking a stable colloidal suspension and reducing its volume by evaporating some of the liquid or reducing the colloidal stability [27].

The electrostatic stabilized gels can be destabilized by changing the process conditions such as the pH of solution. By pH change or if the particle-to-particle distance is reduced by solvent evaporation, the surface charges are decreased and the gelation takes place [32].

In the case of steric stabilization, low coverage of particle surface with polymers may actually lead to flocculation. Flocculation occurs, when the particle has usable an-

choring sites that are not occupied and there are homopolymers, which have a large number of segments. The polymers from a neighboring particle can then attach and form bridges. This type of flocculation is referred to as bridging flocculation [27].

In the case of the depletion stabilization, when the particles approach so close, the pure solvent between the particles will diffuse in to the surrounding region to lower the concentration of the polymer. This would be equivalent to an attraction between the particles, which lead to flocculation [27].

In electrostatic stabilization, flocculation of the sols may also be induced by, reducing the solvency (e.g. by adding a non-solvent) of the polyelectrolytes [30].

3.2 Polymeric sol-gel

Polymeric gels are prepared from liquid precursors through three basic steps: 1) partial hydrolysis of precursors to form reactive monomers, 2) the poly condensation of these monomers to form colloid-like oligomers (sol formation), 3) additional hydrolysis to promote polymerization and cross-linking leading to a 3-dimensional matrix gel formation [28].

As illustrated from Figure 3-4 once the sol is obtained it is then deposited on the substrate, dried and calcined. The following chapter will review all different steps of sol-gel process for application of thin films.
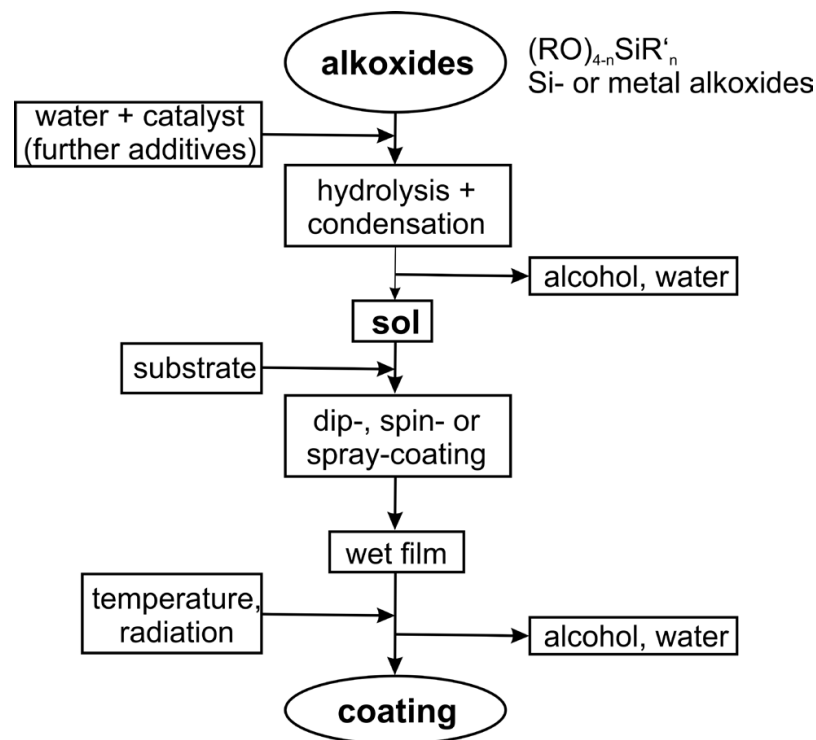

Figure 3-4 Sol-gel processing for coatings [33]

3.2.1 Precursors

The most widely used precursors are metal alkoxides M $(OR)_n$, where M represents a network-forming element such as Si, Ti, Zr, Al, B, etc., and R is typically an alkyl group (C_xH_{2x+1}). The wide application of metal alkoxide in sol-gel process is due to the fact that they are hydrolyzed easily [34].

Mixed-metal alkoxide systems are interesting since they allow tailoring some of the thin films properties enabling their use in widespread applications. When combinations of different metal alkoxides are used, not only the catalyst but also chemical reactivity of metal alkoxides will affect the structure and morphology of the resulting network. The reactivity of metal alkoxides needs to be controlled since the difference in their reactivity can cause phase separation. Among the different alkoxides, silicon alkoxides have the less reactivity while non-silicate metal alkoxides, including elements such as Ti, Zr, Al, and B have much higher reactivity [34]. The sequence of reactivity is expressed as follows:

Zr $(OR)_4$, Al $(OR)_3$ > Ti $(OR)_4$ > Sn $(OR)_4$ >>Si $(OR)_4$

In order to control the co-reactivity of two or more metal alkoxide species and in order to avoid their phase separation some chemical additives such as glycols, organic acids (acetic acid), β-dicarbonyl ligands (ethyl acetoacetate (EACAC)), is used as chelating ligands which can slow down the hydrolysis and condensation reactions of non-silicate metal alkoxide [34].

By combining the inorganic alkoxide moieties with those of oligomeric/polymeric species a new range of material and properties can be produced: hybrid sol-gels. Hybrid coatings are mainly prepared by mixing alkoxide with organic polymers or organo alkoxy-silanes. The organo alkoxy-silanes has a general formula $R'_nSi(OR)_{4-n}$ in which R′ can be any organo functional group and n is generally 1 or 2. Hybrid sol-gels will be discussed in details in Chapter 4.2. Table 3-1 lists a number of different precursors that can be used in sol-gel process [34, 35].

Water plays an important role in the hydrolysis and condensation processes of alkoxides and the molar ratio of water to precursor can affect the structural evolution of sol-gel materials. Increasing Q (water: precursor ratio) leads to an increase in film thickness. At low pH, hydrolysis is relatively faster than condensation so as Q is increased, the extra water promotes hydrolysis and is consumed causing the gel time to become shorter and so thicker films can be formed. If the Q increases so that there is excess water over that required for hydrolysis at a given sol pH, the extra water will dilute the sol which cause longer gel times and thinner films [36].

Table 3-1 Chemical name, empirical formula, structure, and common abbreviation of some of the most commonly used precursors for the preparation of coatings by sol–gel method [35].

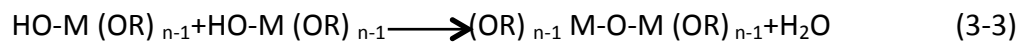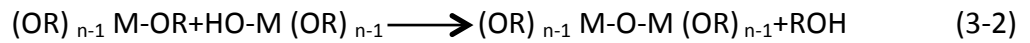| Chemical name	Empirical formula	Abbreviation
Methyltrimethoxysilane	$C_4H_{12}O_3Si$	MTMS
Tetramethylorthosilicate	$C_4H_{12}O_4Si$	TMOS
Vinyltrimethoxysilane	$C_5H_{12}O_3Si$	VTMS
3,3,3-Trifluoropropyltrimethoxysilane	$C_6H_{13}F_3O_3Si$	TFPTMOS
Diethoxydimethylsilane	$C_6H_{16}O_2Si$	DEDMS
Triethoxysilane	$C_6H_{16}O_3Si$	TEOS
C-Mercaptopropyltrimethoxysilane	$C_6H_{16}O_3SSi$	MPTMS
3-Aminopropyltrimethoxysilane	$C_6H_{17}NO_3Si$	APTMS
Methyltriethoxysilane	$C_7H_{18}O_3Si$	MTES
Ethyltriacetoxysilane	$C_8H_{14}O_6Si$	ETAS
Vinyltriethoxysilane	$C_8H_{18}O_3Si$	VTES
Tetraethoxysilane	$C_8H_{20}O_4Si$	TEOS
N-(2-Aminoethyl) 3-aminopropyl trimethoxysilane	$C_8H_{22}N_2O_3Si$	AEAPS
Bis(trimethoxysilyl)ethane	$C_8H_{22}O_6Si_2$	BTMSE
Phenyltrimethoxysilane	$C_9H_{14}O_3Si$	PTMS
3-Glycidoxypropyltrimethoxy-silane	C9H20O5Si	GPTMS
3-Aminopropyltriethoxysilane	$C_9H_{23}NO_3Si$	APTES
C-Methacryloxypropyl-trimethoxysilane	$C_{10}H_{20}O_5Si$	MAPTS
2-(3,4-Epoxycyclohexyl)–ethyltrimethoxysilane	$C_{11}H_{22}O_4Si$	ECHETS
Titanium(IV) tetra-1-propoxide	$C_{12}H_{28}O_4Ti$	TIPT
Zirconium(IV) tetra-1-propoxide	$C_{12}H_{28}O_4Zr$	ZrTPO
Diethylphosphonatoethyl-triethoxysilane	$C_{12}H_{29}O_6Psi$	PHS
Bis-1,2-[triethoxysilyl]-ethane	$C_{14}H_{34}O_6Si_2$	BTSE
2,2-Bis-(4-hydroxyphenyl)-propane	$C_{15}H_{16}O_2$	BPA
3-Isocyanatopropyltriethoxysilane	$C_9H_{21}O_3SiNCO$	ICPTES
Bis-[3-(triethoxysilyl)-propyl]-tetrasulfide	$C_{18}H_{42}O_6S_4Si_2$	BTSTS

3.2.2 Hydrolysis and condensation

Polymeric gels consist of a skeletal network of polymer chains that form by entailment and cross-linking of growing polymer chains or polymer clusters resulting from the hydrolysis, condensation, and polymerization of precursors in solution [27].

The hydrolysis consists of replacing one (OR) group of the alkoxide with a hydroxyl ion (OH) resulting in the release of an alcohol molecule (equation3-1) [28].

$$M (OR)_n + H_2O \longrightarrow HO\text{-}M (OR)_{n-1} + ROH \tag{3-1}$$
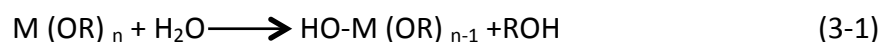
Due to the fact that the alkoxides may be immiscible in water a mutual solvent that is commonly the corresponding alcohol of the alkoxy group, will be used to homogenize the mixture. The process will be continued by polymerization. The polymerization is commonly used in its broadest sense, which means a chemical reaction in which two or more molecules combine to form larger molecules and result in an increase in molecular weight. Polymerization includes condensation which is the reaction between two partially hydrolyzed molecules [HO-M (OR) $_{n-1}$] or one partially hydrolyzed molecule and one alkoxide molecule [M (OR) $_{n}$] to form a M-O-M molecule with a [(OR) $_{n-1}$] attached to each metal atom equation (3-2) and (3-3) [28].

$$(OR)_{n-1} M-OR+HO-M (OR)_{n-1} \longrightarrow (OR)_{n-1} M-O-M (OR)_{n-1}+ROH \qquad (3-2)$$

$$HO-M (OR)_{n-1}+HO-M (OR)_{n-1} \longrightarrow (OR)_{n-1} M-O-M (OR)_{n-1}+H_2O \qquad (3-3)$$

By definition, condensation releases either an alcohol or a water molecule, depending on the initial compounds [37, 28].

In condensation reactions the number of M-O-M bonds will be increased and the number of terminal hydroxyl group will be decreased through internal condensation. Due to addition of monomers, rings will be formed quickly leading to formation of particles [28].

3.2.3 Catalyst

Due to the high reactivity of non-silicate metal alkoxides, generally no catalyst is needed for hydrolysis and condensation. On the other hand, silicon-based metal alkoxides need either an acid or base as catalyst to induce hydrolysis and condensation reactions [28].

The catalysis will affect the sol structure and so allowing control of the final film structure. The final structure of the film will be determined by the size and branching of the polymeric clusters, which are formed through hydrolysis and polycondensation of the precursors [26]. The hydrolysis rate would be higher than condensation under an acidic environment. As a result, acid catalysis promotes the development of more linear or polymer-like molecules in the initial stages that will lead to formation of high-density, low fractal dimension structures. On the other hand, the condensation rate would be higher in the case of base catalysis. Hence, base environment will produce more of a dense-cluster growth that leads to dense, colloidal particulate structures [34].

Inorganic acids, such as HCl, HNO$_3$, H$_2$SO$_4$ and H$_3$PO$_4$ are generally used as acid catalysts. Among these, HCl is the most commonly used which may be due to its lower electronegativity compared to the others [38]. On the other hand, using CH$_3$COOH and NH$_4$OH can cause large amounts of particles precipitation, which makes the formation of film from a stable suspension of oxide particles impossible [39].

3.2.4 Aging

In aging, the prepared sol-gel will be maintained for a period of time, completely immersed in liquid. During aging, polycondensation, syneresis, coarsening and phase transformation processes will occur, singly or simultaneously after the gel point and leads to strengthening, stiffening and shrinkage of the network [4, 27, 36].

The chemical hydrolysis reaction will occur with a very high speed and will be completed in early stages of sol preparation causing large concentration of (MOH) group [28]. Because, concentration of (MOH) group is high, the condensation reaction will be continued and result in an increase in the number of the bridging bonds long after gelation. During aging a more cross-linked structure will be formed, due to losing hydroxyls and formation of new bonds. This process is called polycondensation [4]. When the gel shrinks and ejects the liquid from the pores, syneresis occurs. Syneresis is probably due to condensation between neighboring groups on the surface of the solid network [28]. The coarsening process occurs when a gel is immersed in a liquid in which is soluble. Due to coarsening the average pore size of the gel will be increased while specific surface area will be decrease [4]. Physical properties of the sol such as viscosity, surface tension, evaporation rate of the solvent will determine structure and characteristics of the films [26]. While for some sols, aging is necessary for production of a sol with required characteristics, aging for too long period and at too high temperature leads to gelation before coating. The porosity also can be controlled by, controlling the aging time. For instance, when large porosities are required, aging of base-catalyzed sols can promote growth and agglomeration of particles in the sol, which can result in production of films with high porosity with, pore sizes ranging from nm to tens of nm [36].

As it was mentioned before, due to aggregation that is the result of hydrolysis and condensation, the viscosity of the sol will be increased during aging. As it can be understood from equation (3-4) thickness of coating is proportional to sol viscosity. As the viscosity increases, the thickness of the coating will be increased.

3.2.5 Film deposition

For thin film production, the initial solution or sol containing the precursor is used to coat a substrate by dip coating, spin-coating, spraying or electrophoretic deposition. During film deposition, the structure of the film forms rapidly.

3.2.5.1 Dip coating

In dip coating, a perfect coverage will be obtained as the substrate to be coated is immersed in the sol. The coated substrate will be dragged out at a constant, controlled rate, which results in formation of a uniform film [40]. The gelation process during dip coating process is shown in Figure 3-5.
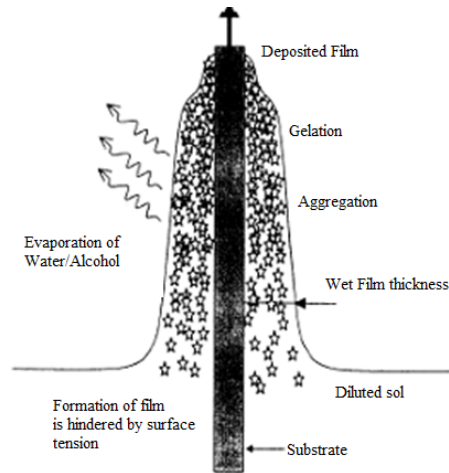
Figure 3-5 Gelation process during dip coating process obtained by evaporation of solvent and subsequent destabilization of the sol [40]

In the next step the glass-like or ceramic films will be densified in an appropriate atmosphere and at temperatures that depends on the thin film composition [26, 40]. Dip coating has some disadvantages such as uneven film thickness particularly at the bottom edge of the substrate [41].

The film thickness and porosity can be controlled by sol viscosity and the withdrawing speed as shown in equation (3-4) [40].

$$d=0.94\ \frac{(\eta U0)^{1/2}}{\gamma LV^{1/6}(\rho-g)^{1/2}} \tag{3-4}$$

In equationU$_0$ is the withdrawing speed, η is the viscosity, $\acute{y}$ is the liquid vapor surface tension, ρ is the density of the liquid and g is the gravitational constant. An increase in viscosity and/or in withdrawing speed leads to an increase in film thickness [40]

3.2.5.2 Spin coating

In spin coating process the substrate spins around an axis, which is perpendicular to the coating area [40]. Spin coating is a four stages process: deposition of the sol, spin up, spin off and gelation by solvent evaporation [27]. The different steps, in spin coating are shown in Figure 3-6.
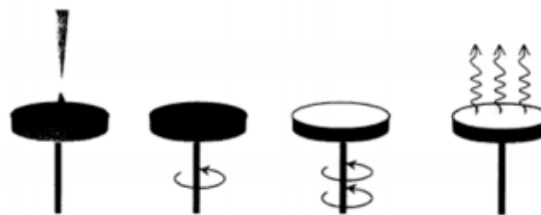
Figure 3-6 Schematic of the stages of the spin coating process: deposition of the sol, spin up, spin off and gelation by solvent evaporation [40]

Many complex reactions such as fluid flow, skin formation, bond formation, striation and solvent evaporation take place during a spin-coating process as shown in Figure 3-7 [41].
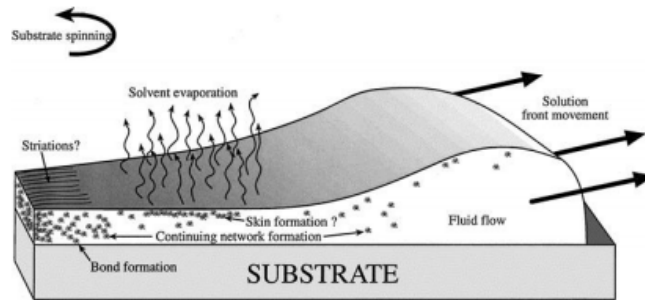

Figure 3-7 Various aspects of the spin-coating process for sol-gel films [41]

During spin coating, centrifugal force will drive the flow radially outward while viscous force (friction) drives it radially inward. The balance between these forces will determine the uniformity of the film [41].

Spin speed is one of the most important factors in spin coating. The degree of radial (centrifugal) force applied to the applied sol as well as the velocity and characteristic turbulence of the air immediately above it, is affected by the speed of the substrate. In particular, the high speed spin step generally defines the final film thickness [41].

3.2.5.3 Spray

In spray coating, the atomizer will turn the sol in to very fine droplets in the nanometer range, which will be dried, and hit the surface. These fine droplets are highly reactive and form a continuous glass film when interacting with the hot substrate surface. A schematic diagram of normal spray technique is shown in Figure 3-8 [40].
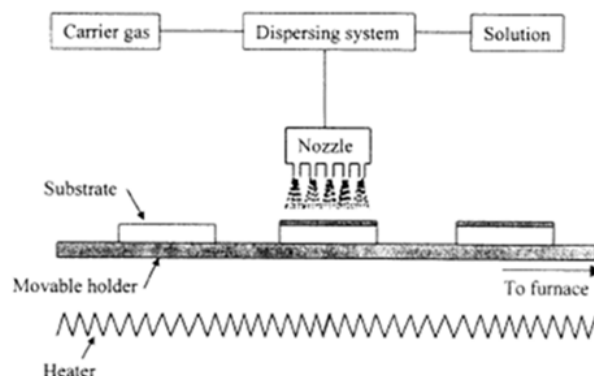
Figure 3-8 Figure 3-9 Schematic diagram of equipment for spray deposition techniques [42]

In comparison with dip coating process, the spraying technique shows some fundamental advantages such as higher speed of deposition, higher flexibility in the shape of

the substrate, lower total amount of coating solution, reduced aging and contamination of the coating solution and availability of the spraying equipment [43].

3.2.5.4 Electrophoretic deposition

Due to the fact that thick coatings can be prepared by electrophoretic deposition, this method has attracted significant attention. Self-supported deposits or thin/thick coatings on conductive or insulator substrates can be manufactured by this method. In electrophoresis deposition process, charged particles in a stable suspension will move when they are subjected to an electrical field. Due to the impact of these particles against a surface with an opposite charge, deposition will occur. A homogeneous coating with controlled thickness can be obtained which are usually denser than those that are made by sol-gel deposition technique [26]. As it can be understood from Figure 3-9 a typical electrophoretic deposition device consists of an electrophoretic cell, the working electrode and the counter electrode.
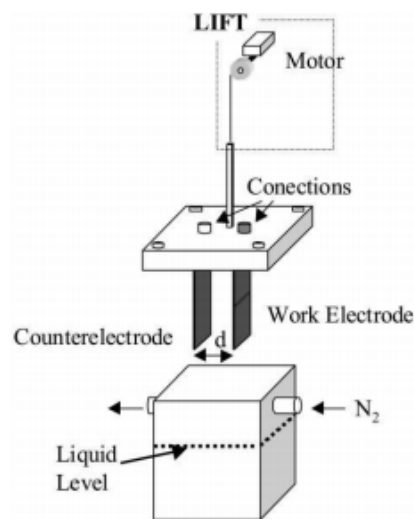
Figure 3-10 Schematic diagram of electrophoretic deposition equipment with rate control [26]

In order to apply a fixed current density a power source is also used and the variation of the potential difference between the electrodes is recorded. The withdrawal rate is controlled by a lift [26].

Electrophoresis offers important advantages such as a short time for formation of a coating, simple apparatus, and no requirement for binder burnout as the green coating contains few or no organics [44].

Versatility of EPD process is due to the fact that, it can be modified easily for a specific application. For example, minor changes in electrode design and positioning can allow film deposition in a large variety of shaped substrate (flat, cylindrical etc.). In EPD the thickness and morphology of the deposited film can be easily controlled through simple adjustment of the deposition time and applied potential [44].

The only intrinsic disadvantages of EPD, is that water cannot be used as the liquid medium. The application of a voltage in water causes the evolution of hydrogen and oxygen gases at the electrodes, which could adversely affect the quality of the deposited film [44].

3.2.5.5 Conclusion

Comparing the advantages and disadvantages of different film deposition methods, it was decided that the dip coating method shall be used for deposition of film on polymeric substrate. Although the main problem with dip coating is the fatty edges forming at the bottom of the substrate, this method remained our best choice. With dip coating the film characterization such as thickness and porosity can be controlled. Furthermore, sides of a substrate can be coated simultaneously with the solution while in spin and spraying coating only one side of the object will be coated by solution.

EPD has not being used in this study. Although by using this method homogenous films, which are usually denser than those from dipping can be obtained but sintering of these deposits requires temperatures excess 1000˚C which limits application of this method for heat sensitive material as substrates [26].

3.2.6 Drying and densification of thin films

After coating, the non-crystalline coating must be dried and densified. Drying in the air or in an oven is a conventional method to remove the excess solvent. In the case of polymeric sol-gels, drying must be carried out slowly and under controlled conditions. Conventional drying of the sol-gel will produce a xerogels. Aerogels are the gels, which are dried under supercritical conditions. No shrinkage occurs in these gels, which result in a structure, which is typically 90 to 95% porous [27].

Densification includes removal of solvent molecules and unreacted organic groups, condensation reactions, structural relaxation and sintering, which is done by using heat. In other words, the free energy of the gel will be reduced during the densification. Furthermore, physical, chemical and structural modifications will take place as gels are heated above room temperature [45, 46].

Drying and densification in furnace has several disadvantages. The whole coated sample (film and substrate) will be heated to the same high firing temperature. However, some substrates such as organic polymers cannot tolerate high temperature exposure [45]. Furnace firing is not capable in production of coated implants with varying surface properties. Furthermore, slower processing time makes the mass productions of thin films a challenge. To overcome the disadvantages of high temperature firing on heat sensitive substrate, the use of laser have been developed. Laser allows locally heating of the coating without heating the substrate [45]. Another solution is to employ hybrid (organic/inorganic) coatings that possess a curing temperature below the temperature at which the substrate undergoes structural modifications [6].

4 LOW CURING TEMPERATURE SOL-GELS AS PROTECTIVE LAYERS OF HEAT SENSITIVE SUBSTRATE

4.1 Titanium dioxide thin films

Biocompatibility, corrosion resistance, high hardness and low tendency to wear are combined in TiO_2 thin films. Compactness, uniformity of the films as well as high interface adhesive strength is very important for improving the corrosion resistance of substrates [47]. Liu et al. showed that TiO_2 and TiO_2-SiO_2 sol-gels films has high electrochemical resistance and can be used as a protective on metallic substrate [48].

The problem with inorganic films that are applied by sol-gel method is the relatively high temperature that is required for their densification (600 °C). This limits application of inorganic sol-gels for heat sensitive substrates such as polymers. In order to solve this problem, absorbed laser radiation can be used for locally heating and thus drying/sintering the coating. Combination of the sol-gel method with laser processing is generally called by the term "sol-gel/Laser-induced technique" (SGLIT). A wide range of advantages aroused when combining laser and sol-gel coating. For instance, the laser parameters such as energy, speed and wavelength can be tailored to control the degree of densification. Thus different properties in different areas of the same coating can be achieved. A pattern can be written into a sol-gel coating by densification with a laser, and the remaining undense coating can be easily etched away to reveal the pattern. One of the laser firing parameters, can be changed continuously as the coated body is fired, producing a film with graded properties. Furthermore, heating the substrate slightly and locally will provide the conditions so that low-refractory materials can be used as substrates. This method is also fast, environmental friendly and production flexible [37, 45, 49, 50]. Figure 4-1 illustrates the CO_2-laser irradiation of titania coatings taken as an example.
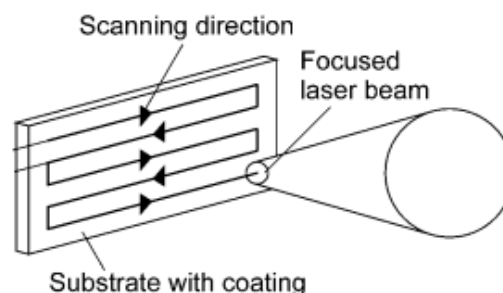

Figure 4-1 CO_2-laser treatment of titania coatings [49]

Two methods for laser irradiation are available for the densification of sol-gel: direct and indirect writing. In direct writing, the sample is directly exposed to laser energy and the patterns are created through absorption of the laser energy by the coating. The sample may move under a stationary beam or the beam may move on the surface of the sample by using a system of mirrors and lenses. In indirect writing method, an absorbing over layer will cover the coating, which is transparent to the laser radiation. This layer absorbs the laser energy, which results in local heating and densification of the sol- gel film [51].

The properties of laser-densified films are different than those of films fired in furnace. This is due to the fact that the heating and cooling are extremely rapid during laser processing of films in comparison with furnace firing [51].

4.1.1 CO$_2$ laser application in sol-gel processing

CO$_2$ laser is preferably employed, due to the fact that for many oxide films and substrates, the 10.6 μm line from a CO$_2$ laser is absorbed by the oxide lattice, enabling heating and densification. Besides, simplicity of operation and being an inexpensive method; CO$_2$ lasers rapidly became a common device in sol-gel densification. Moritz et al. used a CO$_2$ laser to show the influence of laser treatment on crystal structure of the TiO$_2$ coatings by comparing the furnace heat treated TiO$_2$ coatings with the laser-treated ones upon irradiation under various conditions [52]. Figure 4-2 shows the film thickness as a function of firing temperature and laser power.
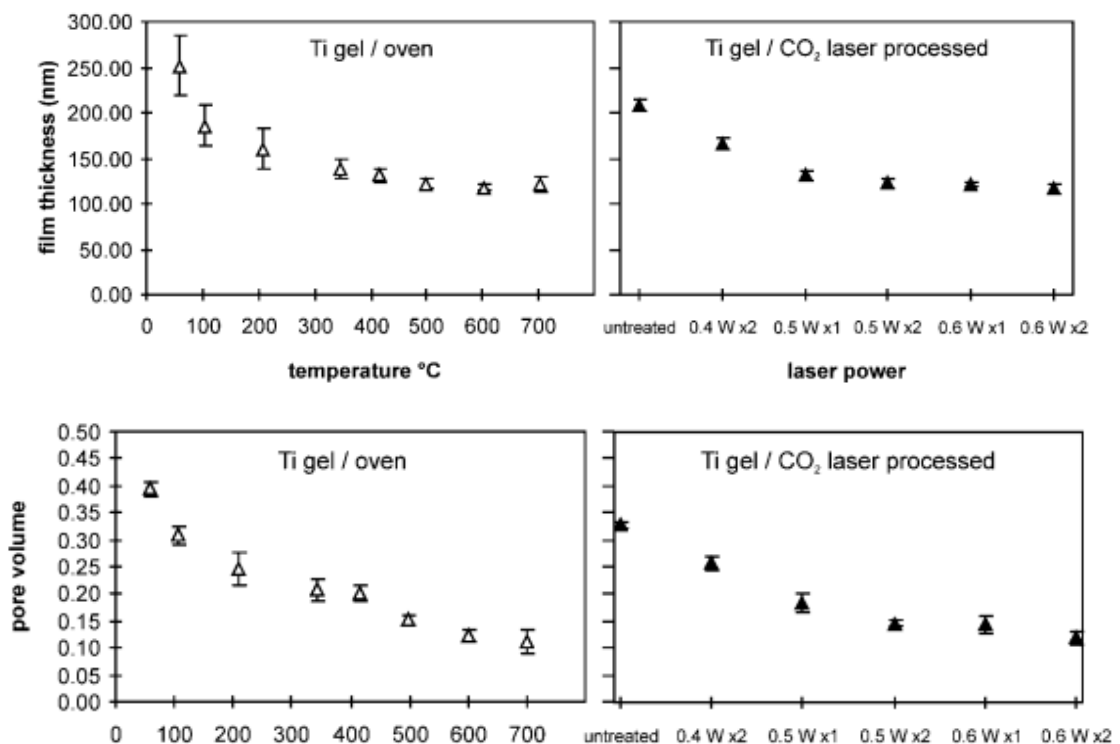
Figure 4-2 Comparison between heat treatments at various temperatures and the direct CO$_2$-laser treatment of one-layersol–gel-derived titania coatings on glass substrates. The laser power range was 0.4–0.6 W, and the treatments were performed once or twice [49]

It can be seen from Figure 4-2 that, the film thickness and porosity of the coatings decreases with increasing the firing temperature. A similar behavior was evidenced when the coating was densified by laser irradiation upon increasing the laser power [49].

This result suggests that CO_2 laser processing had an effect on TiO_2 coatings comparable to that of thermal processing in a furnace [49].

4.1.2 Excimer laser application

Excimer lasers have the capability for producing high-power radiation in the ultraviolet portion of the spectrum which means that diffraction limited focal spot can be even smaller than other high-power lasers. Furthermore, a good coupling of the energy to a work piece can be achieved in the short wavelengths [37]. Since molecules containing the noble gases are used in excimer lasers, no chemical compounds under normal conditions would form. This method is a clean, easy and versatile physical way to stimulate the nucleation and growth of catalytically active crystalline modifications of corresponding oxides [53].

Different photo-irradiation methods can be used as an alternative to conventional heat-treatments for modifying of sol-gel films. They include different excimer lasers with different wavelengths such as F_2 (157 nm), ArF (193 nm), KrCl (222nm), KrF (248 nm), XeCl (308 nm) and XeF (351 nm) [37, 53].

Ultraviolet (UV) photons are expected to result in significant modifications in sol-gel films even at low temperatures since electronic excitations are directly stimulated by the irradiation [54].

Asakuma et al., Starbova et al. and Imai et al. suggested using UV radiation for the annealing of sol-gel films. Asakuma et al. have reported the structural changes in various kinds of sol-gel thin films induced with coherent UV beams. Crystallization behaviors of transition metal oxides were studied using irradiation with ArF, KrF and XeCl excimer lasers. Table 4-1 shows crystallization behaviors of different kinds of samples induced by the laser irradiations.

Table 4-1 The absorption edge, crystallization behavior by UV laser irradiation and the crystallization temperature by calcination in air of inorganic, oxide gel films [54].

Oxide gel films	Wavelength of absorption edge (nm)	Effect of irradiation			Crystallization temperature (°C)
		ArF (193 nm)	KrF (248 nm)	XeCl (308 nm)	
TiO_2	380	-	Crystalline (rutile)	Crystalline (rutile)	400(anatase)
Nb_2O_5	350	-	Crystalline	Crystalline	600
Ta_2O_5	300	Crystalline	Crystalline	Amorphous	700
$SrTiO_3$	320	Crystalline	Crystalline	Amorphous	700
$BaTiO_3$	320	Amorphous	Amorphous	Crystalline	800
$LiNbO_3$	320	-	Amorphous	-	600
$LiTaO_3$	280	-	Amorphous	-	600
PZT	380	(pyrochlore)	(pyrochlore pb metal)	(pyrochlore pb metal)	600(pyrochlore)

From Table 4-1, TiO$_2$, Nb$_2$O$_5$, Ta$_2$O$_5$, SrTiO$_3$ and PZT dried gel films, were crystallized by the UV laser irradiation. On the other hand, the photo-induced structural change in gel films of BaTiO$_3$, LiNbO$_3$ and LiTaO$_3$ was not observed, although these films were thermally crystallized at almost the same temperature as the others [54].

Imai et al. investigated densification of sol-gel derived SiO$_2$ and TiO$_2$ films by UV and VUV light. The coated samples were subjected to energetic photons in the range of 5-18 eV and irradiation of 4.9 eV light produced by low pressure mercury lamp. SiO$_2$ and TiO$_2$ gel films were found to be densified by photons with energies higher than the absorption edge of the gels. So, the changes in structure of gels can be related to rearrangements of the gel structure through electronic excitation [55].

Starbova et al. investigated the effect of KrF excimer laser on the structural and physical properties (structure, phase composition and wettability) of sol–gel titania thin films. The effect of pulses number, on the structure and morphology of the coatings also were investigated [53].

4.2 Hybrid sol-gels

Although inorganic sol-gels are excellent abrasion resistant material and have high density, they are not a good choice as corrosion resistant layers. The major drawbacks of the inorganic sol-gel coatings, as a corrosion resistance layer, is because (1) thick coatings (>1μm) are difficult to achieve without cracking, (2) brittle inorganic films have high crack-forming potential, (3) pure inorganic films have apertures, (4) high temperature processing. These disadvantages make inorganic sol–gel films poor physical barriers, which cannot provide adequate corrosion protection on heat sensitive substrates. On the other hand, traditional polymer coatings systems, are mechanically flexible and tough, but have poor abrasion, adhesion to substrate and thermal resistance [6].

The problem with inorganic and organic sol-gels can be overcome by combining the properties of inorganic and organic material by forming a hybrid network. These hybrid materials are called with different names such as OR-MOSILS (ORganically MOdified SILicates), ORMOCERS (ORganically MOdified CERAMics) and CERAMERS (CERamic polyMERs) or POLYCERAM (POLYmeric CERAM-ics) [56]. Properties such as high transparency (glasslike), low processing temperatures, toughness and elasticity (polymer-like), sufficient thermal stability (silicone-like) and hardness, chemical resistance (inorganic solids) can be achieved by combining the organic and inorganic components [57].

As hybrid sol–gel coatings are applied, strong van der Waals bonds between films and surface will be formed in the first place which will be transformed to stable covalent bonds during drying stage of the films. By introducing organic groups to the sol-gel, the required temperature for calcination of sol-gels can also be reduced. In some particular cases it was reported that drying could be performed at room temperature [6].

There are two methods for preparation of hybrid inorganic-organic sol-gel materials. The first method (class I) includes embedding of organic molecules into an inorganic

material, or vice versa [58]. In this method, only weak bonds exist between both phases. In this regard, the guest molecules can be physically dissolved by the precursors of the inorganic host (e.g., tetraethoxysilane, TEOS, or tetramethoxysi-lane, TMOS) or added to the sol state so they can be entrapped in the gel or xerogels resulting from condensation and drying of the mixture [57].

In the second method (class II) the inorganic and organic components are connected covalently. In this approach, molecular precursors are required which contain a hydrolytically stable chemical bond between the oxide forming element of the inorganic network and the organic moieties. In this regard, alongside the simple metal or silicon alkoxides, which form inorganic oxidic network after hydrolysis, organo (alkoxy) silanes can be used to incorporate polymerizable organic substituents (epoxy, vinyl, or methacryloxy groups) into the final product. The Si-C bonds in organo (alkoxy) silanes are stable under the mild conditions of sol-gel processing and so they are widely used in sol-gel approach [57]. Equation (4-1) shows how a combination of organo (alkoxy) silanes and simple metal or silicon alkoxides can be used for synthesis of class II hybrid sol-gels [58].

$$x\ RE(OR`)_n\ +\ y\ E(OR´)_n\ +\ z\ H_2O\ \longrightarrow R_q\ E\ O_p + w\ R`OH \tag{4-1}$$
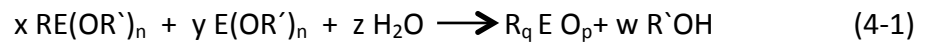
The formula of organo (alkoxy) silanes is $RE\ (OR`)_n$ in which, R is various organic functional groups and E is the element. Organic-inorganic hybrid materials can be modified in various ways. (1) Element E can be changed. In essence, any element E (or combinations of different elements in multicomponent systems) for which compounds suitable for sol-gel processing are available can be used for the formation of the inorganic structures. (2) The organic group R can be changed in organo (alkoxy) silanes. Nearly unlimited choices can be made for organic group R. The only condition that should be considered is that the group should be hydrolytically stable or reacts with water in a controlled way [58].

The properties of organic components and also ratio of inorganic–organic components can effectively influence the corrosion resistance of hybrid coatings. Presence of organic components can increase coating thickness and lower the curing temperature [6].

As it can be understood from equation 4-1 the ratio of the organic and inorganic molecules can be modified. With decreasing x, the hybrid materials become "more inorganic", and vice versa [58]. By increasing of polymer or organic component concentration thicker films would be formed that can restrict the diffusion of potentially corrosive species to the coating/substrate interface. However, a high concentration of polymer or organic component decreases the effect of adhesion and reinforcement of inorganic sol. In other words, an appropriate ratio of inorganic–organic components should be considered to obtain the maximum corrosion resistance [6].

4.2.1 Hybrid sol-gels as corrosion protective layers

Thick coatings limit the diffusion of corrosion species such as water, oxygen and chloride ions to the coating/substrate interface [6]. Organically modified sol-gel systems can provide the opportunity to prepare, thick and crack free coatings [6].

Other studies on corrosion protection by hybrid sol-gels, shows that although these coatings can limit the diffusion of corrosive ions, they cannot eliminate film porosity completely which will allow the electrolyte to reach the substrate and trigger localized corrosion. As a novel approach, the sol–gel coatings can be doped with environmentally friendly inhibitors to improve corrosion resistance. In this method, 'barrier' properties will be combined with active inhibition of corrosion, especially when the integrity of the coating is compromised [26]. Corrosion inhibitors can be even organic or inorganic and can be added to the sol–gel system during a synthesis procedure for pretreatments or at the stage of film formation and cross-linking [6].

Different inorganic inhibitors have been used in order to increase the corrosion protection of hybrid coatings. Phosphates, vanadate, rare earth elements are inorganic inhibitors. Cerium and lanthanum ions can also be used as corrosion inhibitors. The mechanism of corrosion resistance of Ce^{3+} and La^{3+} is based on formation of highly insoluble deposits on intermetallic inclusions. These hydroxide precipitates prevent local increase of pH, which is the main reason for acceleration of the corrosion process. They also act as a diffusion barrier, preventing the corrosion processes to occur in active zones. As it was mentioned before organic inhibitors are also widely being used for corrosion protection. Triazole and Thiazole derivatives, 8-hydroxy quinolone (8HQ), are organic inhibitors, which have been used for corrosion protection of aluminum alloy. In the case of 8-hydroxyquinoline on pure aluminum the improvement in the corrosion protection is explained by formation of a complex aluminum chelate on the surface [6].

Table 4-2 shows some of the recipes reported in the literature on the corrosion resistance and biocompatibility of hybrid sol-gels. Some of the other recipes have been reviewed by Figueira et al. [35].

Table 4-2 Studies on corrosion protection using Hybride sol-gels

Precursors	Curing Temperature/ duration of heating	Results and conclusions	Biocompatibility Test	References
TMOS, MAPTMS	120˚C/2h	Hybrid coatings containing HA particles show higher thermal stability, greater thickness and were more hydrophobic than coatings without HA. The coatings were effective physical barriers and could improve corrosion protection.	Biocompatible	[13]
TEOS, MPS	300˚C/0.5h	Uniform, defect-free and relatively dense coating was obtained. The hybrid coatings on stainless steel substrates could improve the corrosion protection. SiO_2-MPS hybrid coatings are promising candidates for biocompatible applications.	Biocompatible	[59]
TEOS, MTES GPTS	130˚C / 1h	Addition Aerosil particles to epoxysilane coatings can improve the protection properties	No test	[60]
TEOS, MAPTS	37˚C /24 h	The sol-gel improves the corrosion resistance of 316L steel in physiological Medium for biomedical applications.	Biocompatible	[61]
GPTMS, TMOS	100˚C /5 h	Hybrid coating showed good corrosion resistance	No test	[62]
GPMEOS, TEOS	Room temperature/24 h	Coatings exhibited a good anticorrosion performance using cerium nitrate inhibitor	No test	[63]
APTES, APTMS, GPTMS, TMSPh	150˚C/1.5 h	The Hybrid coatings showed significant corrosion resistance based on APTMS and APTES	No test	[64]
MAPTS, MPTMS, SiO2	150˚C/0.5h	Corrosion protection is provided, by sealing the pores in the anodized layer, acting as a barrier. The multilayer sol-gel eliminated the diffusion paths for corrosive species.	No test	[65]
ZrTPO, GPTMS	130℃ /1 h	Inhibitor-doped hybrid sol–gel coatings were synthesized by addition of corrosion inhibitor 8-HQ to the sol–gel films. The inhibitors improved the protective properties of the film significantly.	No test	[66]
GPTMS, MTES	150 ℃ /2 h	Surface conditioning process is a key step to achieve the required anti corrosion properties of Hybrid coatings.	Biocompatible	[67]
GPTMS, TMOS	100℃ /5 h	Hybrid coatings doped with inhibitor (2-methylpiperidine) showed better corrosion resistance than undoped coating.	No tests	[68]
TMOS, DEDMS	100℃ /1 h	Sol–gel coatings provide corrosion protection but they have not defined barrier properties. Organic–inorganic coatings provide better corrosion protection than inorganic ones. Hybrid coatings doped with Ce^{3+} was effective as pretreatments for a final acrylic coating.	No tests	[13]
GPTMS, VTES	100℃ /1 h	Increasing of $[Ce^{3+}]$ on the Hybrid coating decreases the anticorrosion effect	No tests	[69]
TEOS, GPTMS	100℃/0.5 h	Study of the Hybrid films properties, characterization and formation mechanism.	No tests	[70]
MAPTS, TMOS	40℃/6 days	Anticorrosive performance of the Ce^{3+} ions trapped within the Hybrid network.	No tests	[71]

4.2.2 Coating of organic polymers by sol-gel derived hybrid materials

The unique properties of polymers such as lightweight, optical transparency, electrical and mechanical properties and ease in mass production have expanded their applications in both everyday life and high technologies [41]. However, their applications have been limited, due to their relatively low abrasion and wear resistance and environmental degradation [41].

One approach to overcome these limitations is to apply hybrid coatings on substrates through various sol-gel techniques. As it was mentioned before, applying hybrid coatings by dip coating of sol-gel allows manipulating the chemical composition and controlling the thickness of the coating by changing the substrate withdrawal rate and organic-inorganic ratios [40, 6]. In addition, hybrid sol-gels can be heat treated at low temperatures so this technique is perfectly suited for coating polymers, which usually have limited thermal stability [6].

4.2.2.1 Polymeric substrates

It should be considered that chemical make-up and structure of various polymers are very different, and so the nature of the solution/substrate interactions will be also different. In inorganic sol-gel processing, the main mechanism of adhesion between coating and substrate is through condensation of hydroxyl groups. Since polymeric surfaces do not contain large concentrations of hydroxyls, bonding via condensation of hydroxyl groups can reveal problematic, but other bond mechanisms may occur. One of the advantages of sol-gel hybrids is that radical or UV polymerization can be used in the construction of the hybrid network. This may improve compatibility with the surface of the polymer [41].

The wetting behavior of polymeric surfaces which make them difficult material to be coated by oxide or oxide-based coatings can be improved by surface treatment or modification. Two techniques shown to be effective for modifying the polymer surface include oxygen plasma treatment and wet chemical routes. Other treatments of the polymer surface are possible, such as chemical treatments that can activate the surface of the polymer. IR treatment of polymers may also be used to improve adhesion [41].

Figure 4-3(a) schematically shows the formation of hydroxyl groups on the surface of a polyester substrate after etching. Figure 4-3(b) shows the incorporation of the hybrid coating to the surface of the polyester substrate. In this case, the reaction between hydroxyl groups on the surface of substrate and partially hydrolyzed and/or condensed TEOS sol would form Si-O-C bonds attaching the hybrid coating with the polymer substrate at the interface [72].
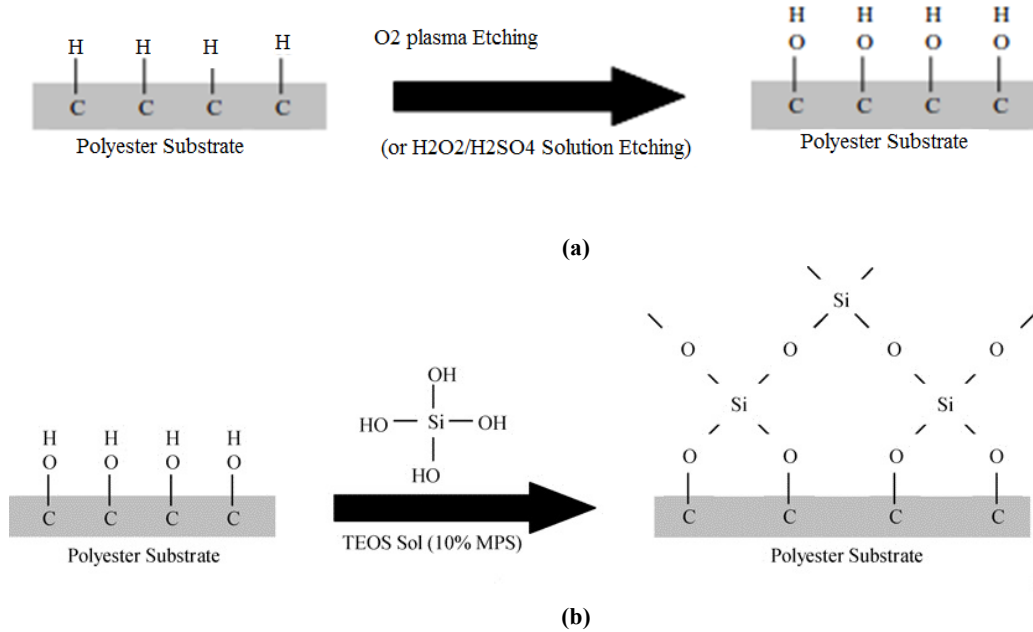
Figure 4-3 Schematic of (a) surface hydroxylation of polyester by way of oxygen plasma etching or hydrogen peroxide and sulfuric acid wetchemical etching, and (b) subsequent attachment of sol-gel-derived hybrid coating on polyester after surface preparation [72].

4.2.2.2 Some factors governing coating of organic Polymers

Difference in modulus and thermal expansion coefficient of coating and substrate are important characteristics since they may lead to failure of the coating under stress or thermal treatment [41]. Because of difference in modulus of the coating and polymeric substrate, the coating may be damaged due to the excessive deformation of substrate. The differences in thermal expansion coefficient between the polymer substrate and the hybrid coating also can cause stresses in the film. The strength of the interfacial bond between the substrate and coating should be greater than the maximum predicted stress faced during temperature variations, caused by unequal thermal expansion coefficients [41].

Solubility of the coating materials and the substrate also should be investigated. If they have radically different solubility in a given solvent, their ability to bond to one another is small and adhesion will be low. On the other hand, adhesion mechanisms can occur if they have similar Van der Waals bond content [41].

5 MATERIALS AND METHODS

5.1 Fabrication and design of substrate

In this thesis, the substrate PLA sheets are made of PLA (Purac Corbion Purasorb PLD962). Granules are melt-processed into a 10 mm diameter rod. Successively, the rod is cut to smaller pieces and compressed to 500 μm thick sheets by using elevated temperature and simultaneous pressure. One side of the polymer is compressed against glass sheet to make the surface of the polymer smooth enough for the evaporation process. Finally, the sheets are cut to 40 mm by 30 mm pieces. The magnesium is patterned, by using physical masks during the evaporation process. In this case, the masks were created by extrusion type 3D printing [1]. Figure 5-1 shows (a) The magnesium patterned PLA sheet, and (b) the cross-section of the resonator structure.

(a) (b)
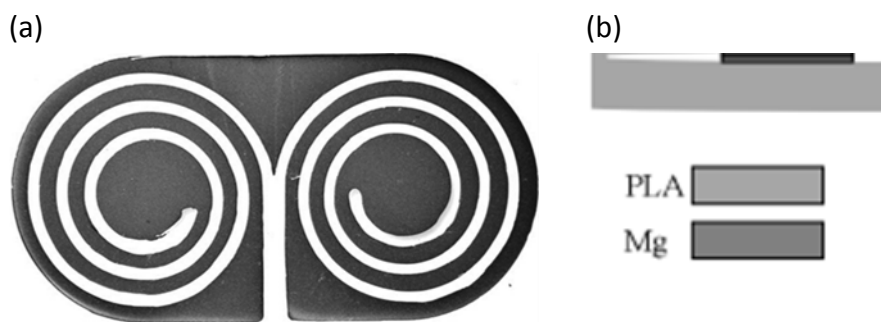
Figure 5-1 (a)The magnesium patterned PLA sheet, (b)The cross-section of the resonator structure[1]

5.2 Sol preparation and film deposition

The effect of three different types of sol-gels (inorganic and hybrid) was investigated on the polymeric substrate.

The first sol-gel which will be called sol A was made by mixing of 2-propanol (Merck), Eacac (Merck), HNO_3 (Merck), Tetra-n-butyl orthotitanate (Merck) and water in order and with volumetric ratios of 40:2:0.25:5:1(ml). The sol was aged for one hour at room temperature while stirring.

The substrates were washed ultrasonically for 5 min in ethanol and dried at room temperature .In this regard ultrasonic bath (Finn Sonic V011) was used. In the next step, the substrates were immersed in to the sol for one minute, slowly extracted vertically at constant rate of (150mm/s). The coated samples were dried at 60˚C during the night and irradiated with various laser parameters.

Figure 5-2 shows schematically the process of inorganic sol-gel preparation and thin film application.
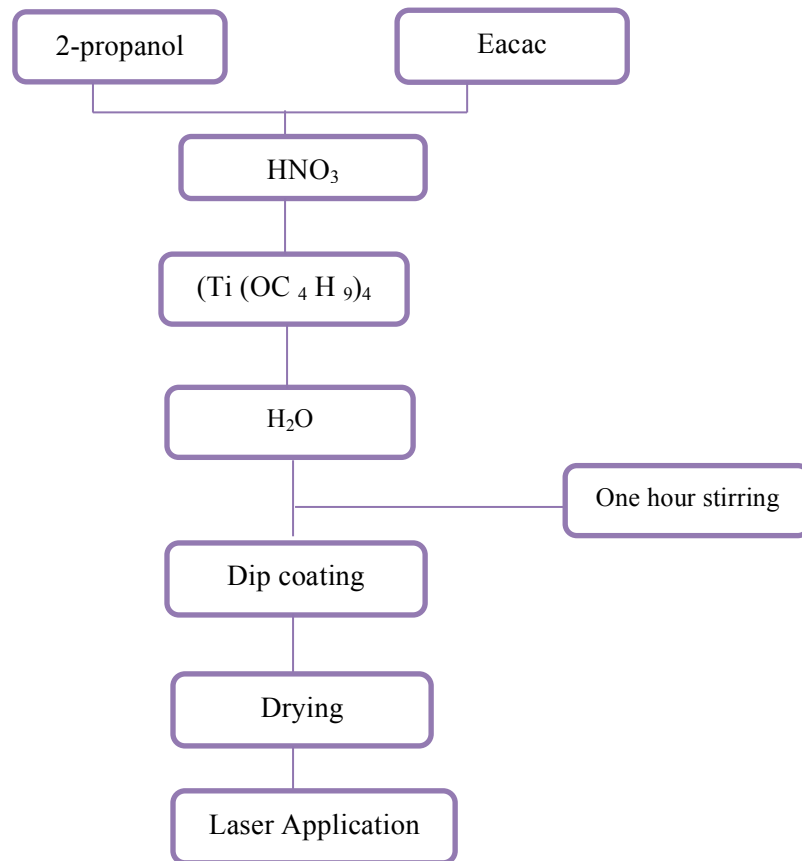
Figure 5-2 Schematic diagram of TiO_2 Sol-gel preparation

The second sol-gel is called sol B that is a mixture of γ-methacryloxypropyltrimethoxysilane 98% (MAPTMS) and tetramethoxy silane 98 % (TMOS) from Aldrich as organopolysiloxane matric precursors at a molar ratio of 4: 1. Ethanol (99.8%) and ddH_2O were used as solvents with MAPTMS hydrolysed with H_2O through stirring, mixed with TMOS vigorously and stirred (700 rpm, 4h). The molar ratio of silane–water–ethanol was 1: 3: 3.

The third sol-gel, which will be called sol C, was made from Mixtures of γ-methacryloxypropyltrimethoxysilane 98% (MAPTMS) from Aldrich and titanium butoxide (Tetra-n-butyl orthotitanate) from Merck. Ethanol (99.8%) and ddH_2O were used as solvents with MAPTMS hydrolyzed with H_2O through stirring, mixed with titanium butoxide vigorously and stirred (700 rpm). The molar ratio of silane–water–ethanol was 1: 3: 3.

Within this sol-gel several parameters were changed to enhance the corrosion resistance ability of the coating.

1. The ratio of MAPTMS/ titanium butoxide was varied from 1:1 to 4:1
2. The samples were dip coated after 4 and 24 hrs of stirring and cured at 60 and 80°C.

For the deposition, all substrates were immersed into the sol for one minute and then slowly extracted vertically at constant rate of 5mm/s.

Figure 5-3 illustrates the sol-gel preparation and thin film application process schematically.
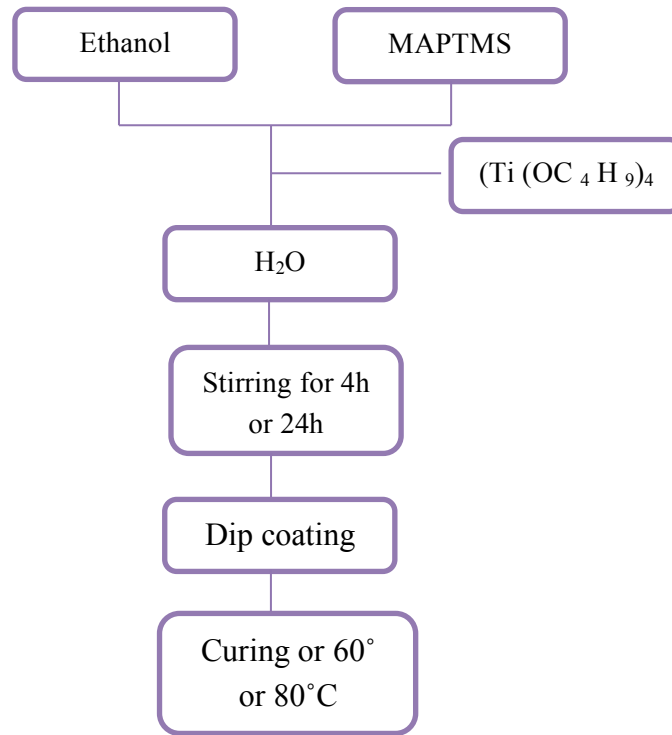
Figure 5-3 Schematic diagram of hybrid sol-gel preparation

Table 5-1, shows a list of different sol-gel films that was prepared a in this study.

Table 5-1 List of prepared films and labels

Sol-gel label	Molar ratio of precursors	Aging	Heat treatment
A	Titanium butoxide	1h at RT	Laser
B	MAPTMS/TMOS: 4/1	4h at RT	80˚C during the night
C	MAPTMS, Titanium butoxide: 4/1	4h at RT	80˚C during the night
4/1, 4(h), 80˚C	MAPTMS/Titanium butoxide: 4/1	4h at RT	80˚C during the night
4/1, 4(h), 60˚C	MAPTMS/Titanium butoxide: 4/1	4h at RT	60˚C during the night
4/1, 24(h), 80˚C	MAPTMS/Titanium butoxide: 4/1	24h at RT	80˚C during the night
4/1, 24(h), 60˚C	MAPTMS/Titanium butoxide: 4/1	24h at RT	60˚C during the night
1/1, 4(h), 80˚C	MAPTMS/Titanium butoxide: 1/1	4h at RT	80˚C during the night
1/1, 4(h), 60˚C	MAPTMS/Titanium butoxide: 1/1	4h at RT	60˚C during the night
1/1, 24(h), 80˚C	MAPTMS/Titanium butoxide: 1/1	24h at RT	80˚C during the night
1/1, 24(h), 80˚C	MAPTMS/Titanium butoxide: 1/1	24h at RT	60˚C during the night

5.3 Dip coating

In this thesis, dip-coating technique was used to apply the coatings. A universal testing machine (INSTRON 4411) was used to perform dip coating. The substrates were dipped in to the sol for 60 seconds. The substrates were withdrawn at the speed of 150 mm/s in case of TiO_2 and 5 mm/s in case of hybrid sol-gels.

5.4 Atomic force microscopy

The surface morphologies of the samples were characterized using an atomic force microscope (XE-100, Park Systems Corp, and USA). The probe was supported on an AP-PNANOTM AFM cantilever (Type: ACTA, L: 125 µm, tip-radius: < 10 nm, f = 200-400 kHz, spring constant: 25-75 Nm^{-1}; coating aluminum). The scan rate was 1 Hz. The surface roughness average (Rq) was calculated from the roughness profile determined by AFM with XEI image processing software (Park Systems). The surface roughness was measured as Root Mean Square (Rq) on a 10µm x 10µm area. Rq is the root mean square average of the measured height deviations, taken within the evaluation length or area and measured from the mean linear surface. The measurement was repeated 4 times on various areas of each sample in non-contact mode, under air and at RT. The Rq values then were then averaged.

5.5 Scanning electron microscopy (SEM) observation

In this study, a SEM was used to observe the topography of the samples. SEM imaging was performed by FESEM (Zeiss ULTRA plus). The extra high-tension voltage was set to 5 KV. The working distance was set to 5.6mm, and the image was obtained using secondary electrons. For the sample topography images, the samples were attached to aluminum stubs with carbon glue and before SEM analysis they were carbon coated to avoid sample charging during SEM.

5.6 Laser application for condensation of sol-gel

In order to sinter the sol-gel locally, absorbed laser radiation was used. The condensation of the sol-gel was performed by a Nd: YAG laser, working at wave length of 1062 nm. The laser was used in continuous wave mode (CW) with average power of 85W, pulse energy of 3.4mJ and pulse duration of 2-500 ns. Effects of different laser parameters such as laser power, speed, distance between the hatches and focus, on densification of a purely inorganic TiO_2 sol were investigated.

5.7 Preparation of simulated body fluid (SBF) and immersion test

The simulated body fluid (SBF) was prepared by dissolving reagent chemicals of NaCl, NaHCO$_3$, KCl, K$_2$HPO$_4$.3H$_2$O, MgCl$_2$.6H$_2$O, CaCl$_2$.2H$_2$O, Na$_2$SO$_4$ and Tris (hydroxymethyl) amino methane into deionized water, as shown in Table 5-2. The fluid was buffered at physiological pH 7.40 at 37˚C with hydrochloric acid.

Table 5-2 Reagents for preparing the simulated body fluid

Order	Reagent	Amount /1 dm^3(H$_2$O)
1	NaCl	7.996
2	NaHCO$_3$	0.353
3	KCl	0.224
4	K$_2$HPO$_4$.3H2O	0.228
5	MgCl$_2$.6H$_2$O	0.305
6	1N-HCL	35(ml)
7	CaCl$_2$.2H$_2$O	0.368
8	Na$_2$SO$_4$	0.071
9	Tris	6.057

In order to evaluate the corrosion resistance, both the uncoated and coated samples were immersed in SBF (pH 7.4) for different immersion periods (6, 24 and 72 hours) in a Termaks incubator in static mode set to 37˚C. The volume of SBF was calculated based on a volume-to-sample area ratio of 50 mL/ cm^2 and SBF was not refreshed over the immersion period. For each time point of the immersion tests, one sample was soaked for morphological observation and one sample was immersed for evaluating the corrosion rate.

5.8 Attenuated total reflectance-Fourier transform infrared (ATR-FTIR) spectroscopy (measurements)

To understand the effect of precursor molar ratio, aging time, curing temperature and number of layers, the chemical structure of the all sample surfaces were studied by ATR-FTIR.

ATR-FTIR measurements of the samples were carried out using a FTIR spectrometer (Perkin Elmer Instruments, Spectrum One, USA). Diamond was used as the crystal in this device. The samples were analysed in the reflectance mode in the range of 600-4000cm^{-1}. For each spectrum, eight scan were accumulated at a resolution of 4cm^{-1}.

5.9 Contact angle measurements

The surface wettability of samples was measured at RT using a theta optical tensiometer (Biolin Scientific). A water droplet was placed on the dry surface of the sample, photographed exactly at the time when the water and the surface enter in contact. To measure the contact angle, a tangent was applied at the spot where the drop met the surface of the substrate. The measurements on the surfaces were carried out four times on each sample and averaged.

5.10 Optical microscopy

In this work, an optical microscope Olympus BH2-UMA was used to define the presence of cracks at the surface of the coated samples prior to immersion in SBF. Since the samples were not transparent an external light source Olympus TGH, was used to shine the light from the top of the sample. Samples were investigated with 5 and 40X magnification.

5.11 Differential scanning calorimetry

In order to estimate the maximum temperature that the substrate can withstand without extensive structural and crystallographic modification, thermal properties of the substrate was investigated by TA (Q1000). Nitrogen was used as a sweeping gas. The sample was cooled to $0\,℃$ in the first place and then heated up to $220\,˚C$ at a rate of $20\,˚C$ / min. In the next step, the sample was cooled down to $0\,℃$ at $50\,˚C/$ min before being heated up a second time to $220\,˚C$ at a rate of $20\,˚C$ / min.

6 RESULTS AND DISCUSSION

6.1 Substrate properties

In this research project the challenge lies in defining a coating that will provide corrosion resistance. The various steps for the production of a corrosion resistant coating are: 1. sol processing, 2. sol deposition and 3. sol drying and densification. Densification is, usually, done by using heat to remove solvent molecules and unreacted organic groups. Condensation reactions along with structural relaxation and sintering will be followed after densification [45, 46]. The heating of the coated substrate usually occurs in a furnace which implies that the whole coated sample, are heated to the same high firing temperature. In general, the substrate thermal properties will dictate the maximum temperature at which the coating can be cured. In our particular case Mg deposited on a PLA substrate will be the sample to be coated. Figure 6-1 shows the DSC thermogram of the polymeric substrate.
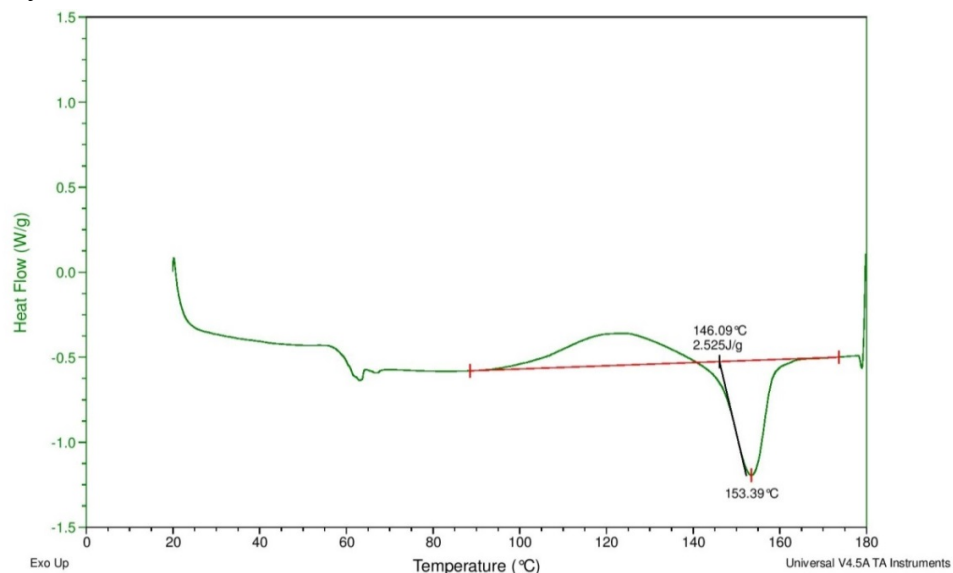
Figure 6-1 DSC thermogram of the PLA substrate

From Figure 6-1 an endothermic event occurs at around 60°C. Such event is typical of the glass transition temperature. Then an exothermic peak related to the cold crystallization exhibit a maximum at about 120°C. Finally the endothermic effect related to the melting of the polymer is seen to have a minimum at 153°C. Thus in order to dry our coating without inducing structural or crystallographic modification, thermal treatment can only been conducted in the $50\text{-}90^{\circ}$C region, where 90°C represent the onset of crystallization, T_x. However, one should keep in mind that at temperature between T_g and T_x softening of the substrate may occur.
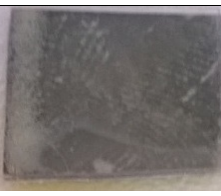
On the other hand, low water contact angle on Mg side of the substrate shows a high wettability of uncoated substrate (of 55˚), which will result in reaction of magnesium layer with water and its break down.

From above explanations, it can be concluded that a coating with capability of being cured at low temperatures and lower the surface wettability of substrate is required. In this regard, local densification of inorganic TiO_2 sol-gel and using hybrid sol-gels will be investigated.

6.2 Laser dried inorganic coatings

In order to overcome the low curing temperature useable on PLA substrate, densification, using irradiation was attempted. In this study, a laser with wavelength of 1062 nm (Nd: YAG laser) was used in direct writing. Effects of different laser parameters such as laser power, speed, distance between the hatches and focus, on densification of a purely inorganic TiO_2 sol (see sol A in section 5.2) were investigated. Table 6-1 presents the list of experiments performed using laser irradiation based on the power, speed and hatches used in direct writing. In all test the beam was focused at the surface of the sample.

Table 6-1 Laser in focuse ,at different powers at the same speed and hatches

Power (w)	speed (mm/s)	Hatches (μm)	Result
60	30	15 -	
10	30	15	
5	30	15	
1	30	15	
3	30	15	

One can note that regardless of the parameter used, the Mg layer does not withstand the laser exposure and consequently degrades.

Table 6-2 shows a set of irradiation performed at various powers while the laser is focused at 5 or 10 mm above the coating surface.

Table 6-2 Effect of laser at different powers and out of focus
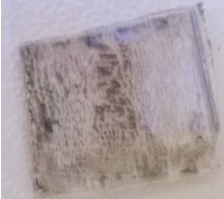
Power (W)	Speed (mm/s)	Hatches (μm)	Out of focus (mm)		
5	30	30	5	10	
3	30	30	10		
2	30	30	10		

Here again all materials, regardless of the power or focus points looked similar, i.e. the Mg layer is being deteriorated by the laser.

Finally, the effect of different laser powers and speeds while the laser is out of focus are reported in Table 6-3.

Table 6-3 Effect of laser at different powers, out of focus and different speeds

Power (w)	Speed (mm/s)	Hatches (μm)	Times	Focus (mm) above the surface	Results
5	1000	30	10	10	
3	1000	30	10	10	
5	500	30	10	10	

Changing the speed of passage of the laser does not allow the coating to be densified without destruction of the Mg layer.

As it can be understood from Table 6-1, 6-2 and 6-3 by applying different laser parameters the Mg-layer has absorbed all the laser power and consequently melted. This is due to the fact that sol A that is a titanium dioxide sol-gel, is transmitting the radiation at the wavelength of 1.06µm. The radiation is absorbed by the metallic layer and causes an increase in temperature, which will result in melting of the substrate.

Figure 6-2 shows transmittance spectra in visible and ultraviolet regions of dried gel films of TiO₂. From the Figure, it can be understood that the thin TiO₂ films can absorb the radiation in ultra violet region. On the other hand, these films are transparent in visible region.
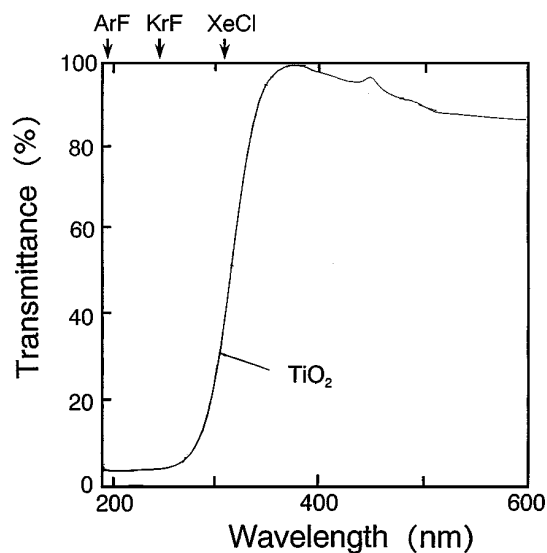
Figure 6-2 Transmittance spectra in visible and ultraviolet regions of dried gel films of TiO2

The desired heating of the sol-gel film can be obtained when the film and/or substrate absorb the laser operating wavelength or alternatively, an absorbing metal cladding is deposited on the top of the film [73]. Titania films absorb in the UV and IR spectral region; therefore, suitable laser source candidates are excimer lasers (in the UV) and CO₂ lasers (emitting in the IR at 10.6 µm). Nd: YAG lasers, emitting in the NIR at 1.06µm, require the use of adsorbing metal claddings. Figure 6-3; illustrate the indirect laser writing that should have been used for densification of sol A using a Nd: YAG laser [73].
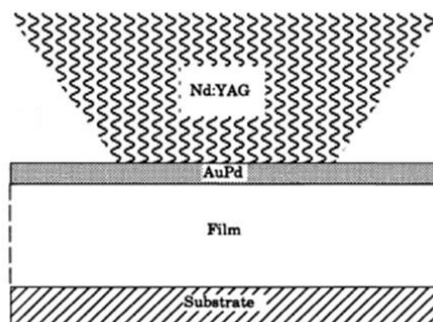
Figure 6-3 metal coated sol-gel/laser coating using a Nd:YAG laser [45]

6.3 Hybrid coatings

As low densification temperature cannot be reached with typical inorganic coatings and because laser with suitable wavelength were not readily available, the use of a hybrid (inorganic/organic) sol-gel appeared to be the solution. As presented in Table 4-2 in section 4.2.1, some organic/inorganic hybrid sol-gels exhibit low densification temperature.

In a first time we attempted developing two inorganic/organic sol-gels: one based on silicon dioxide and one based on titanium dioxide. Sol B (made from Mixtures of γ-methacryloxypropyltrimethoxysilane 98 %(MAPTMS) and tetramethoxy silane 98% (TMOS) and sol C (made from Mixtures of γ-methacryloxypropyltrimethoxysilane 98% (MAPTMS) and titanium butoxide (Tetra-n-butyl orthotitanate) were dip coated at the surface of the substrate and dried at 60˚C overnight. Figure 6-4 shows pictures of the coated samples after they have cooled down to room temperature.

(a)   **(b)**
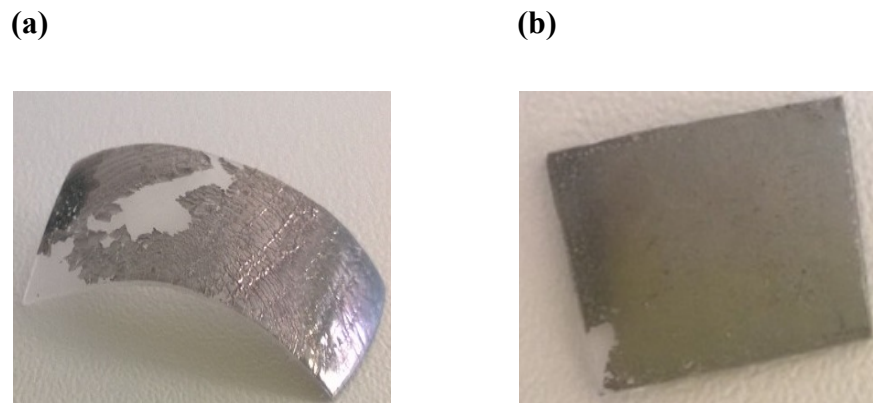
Figure 6-4(a)Sol B (b)Sol C

The sample, which was coated with sol B, was bended extensively and the magnesium layer was removed. This, most likely, happened due to the difference in modulus of the coating and the polymeric substrate. In this regard, the magnesium layer and applied film may be damaged due to the excessive deformation of the substrate. The differences in thermal expansion coefficient between the polymer substrate and the hybrid coating also can be another reason which cause stresses in the film and result in bending of substrate [41].

From Figure 6-4(b), it appears that the hybrid sol-gel containing titanium exhibit the best compatibility with the PLA substrate and thus should protect more efficiently the Mg layer at the surface of the PLA. Therefore, in the next steps the effect of different parameters such as aging time, curing temperature, number of layers and different ratios of MAPTMS/titanium butoxide will be investigated.

6.4 Effect of curing temperature, aging time, different ratios and the number of layers

The effect of curing temperature, aging time and different ratios on the surface quality, surface roughness, contact angle, chemical structure and corrosion resistance of the films were investigated.

As it was mentioned in Chapter 5, effect of two different ratios of MAPTMS/titanium butoxide was investigated in sol C. These two different ratios were labelled as 4/1 and 1/1 in this thesis. The samples were also either cured at 60˚C or 80˚C. It was also aged either for 4(h) or 24(h). The samples were labelled base on MAPTMS/titanium butoxide ratio, aging hours and curing temperature. In case of samples with five layers the samples are labelled with MAPTMS/titanium butoxide ratio, curing temperature.

6.4.1 Wetting of the substrate

Wettability studies usually involve the measurement of contact angles as the primary data, which indicates the degree of wetting when a solid and liquid interact. Small contact angles (<90°) correspond to high wettability, while large contact angles (>90°) correspond to low wettability [74]. In order to understand if the sol C processed with various parameters is capable of wetting the surface of sample, a droplet of each sol was placed on both dry surfaces (Magnesium and PLA side) of uncoated sample. Figure 6-5 shows the photo images of sol drops of (a) 4/1 sol, on magnesium side (Θ=12˚) (b) 4/1 sol, on PLA side (Θ=28˚) (c) 1/1 sol, on magnesium side (Θ=14˚) (d) 1/1sol, on PLA side (Θ=23˚).
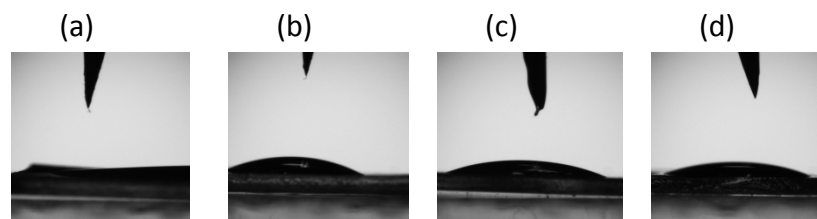
Figure 6-5 Photo images of sol drops of 4/1, on Magnesium side of sample (a) 4/1,on PLA side of sample (b) 1/1, on Magnesium side of sample (c) 1/1,on PLA side of sample(d).

Comparing the results revealed that both 4/1 and 1/1 sols are capable of wetting the sample surfaces perfectly. The magnesium side exhibit higher wettability in comparison with the PLA side of the sample.

6.4.2 Surface roughness

The surface morphology of modified sol C was studied by atomic force microscopy (AFM). The surface roughness was measured as Root Mean Square (Rq) on a 10μm x

10µm area. The measurement was repeated 4 times on various areas of each sample and the Rq values averaged.

Figure 6-6 presents the AFM image of the uncoated sample a) and the thin films with a ratio MAPTMS/titanium butoxide 1/1, aged for 4h and cured at 60˚C labelled 1/1, 4(h), 60˚C b); 1/1 4h; 80˚C c), 1/1 24(h) 80˚C d) as well as samples coated with 5 layers 1/1, 60˚C e) and 1/1, 80˚C f).
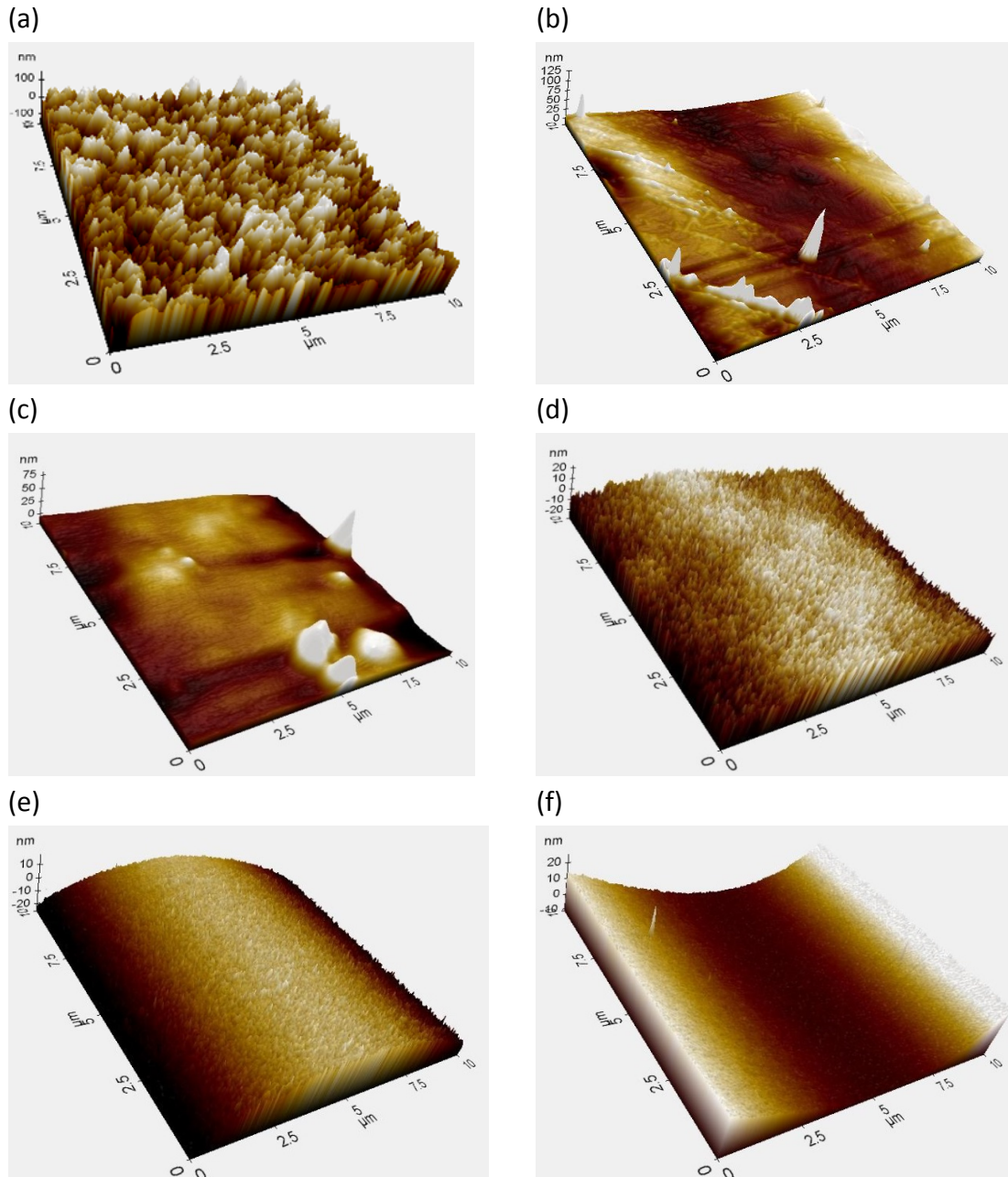

Figure 6-6 AFM images of uncoated (a); 1/1, 4(h), 60˚C (b); 1/1 4h; 80˚C (c), 1/1 24(h) 80˚C (d); 1/1, 60˚C (e);,1/1, 80˚C (f)

Comparisons of the Rq values as a function of the sol-gel preparation parameters are provided in Figure 6-7.
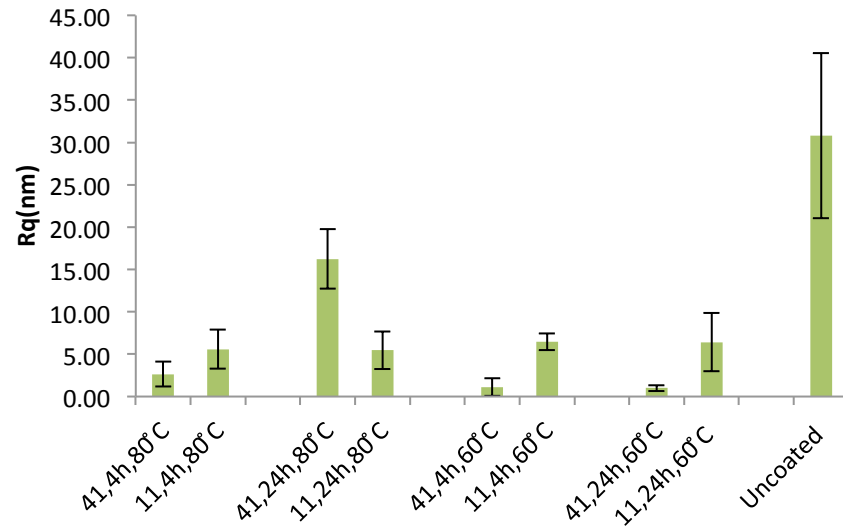
Figure 6-7 Average R_qs and their deviations of one layer film from Sol C at different MAPTMS/Titanum butoxide ratios,Temeratures and aging time . The data are averaged values from totally 4areas of 10 μm^2

From Figure 6-7, The Rq value for the uncoated sample (30.81±9.75 nm) is much higher than the values obtained for the coated samples. This indicates that the coating has provided a smooth and even surface on the substrates. It also appears that when using similar parameters the coatings with MAPTMS/titanium butoxide ratio 1/1 shows always slightly higher roughness, except for the sample 4/1, 24h, 80˚C. It is thus assumed that this belongs to an experimental error. The surface roughness is assumed to increase with increasing the inorganic part in the hybrid sol-gel [75]. More open/porous structure appears in the hybrid sol-gels with higher Rqs [76]. Therefore, for the hybrid sol-gel with higher MAPTMS content (MAPTMS: titanium butoxide =4:1) smaller pores are expected.

It can also be noticed that effect of aging time on roughness is insignificant. Curing temperature effect the surface roughness of the samples with different MAPTMS/titanium butoxide ratios differently. In case of samples with 4/1 ratio, the ones, which have been cured at 80˚C, show a higher roughness in comparison with those cured at 60 ˚C. This behaviour is reverse in case of samples with 1/1 ratio. It can be concluded that 4/1 samples which are cured at 60 ˚C and 1/1 samples, which are cured at 80˚C, show a lower porosity and crack forming potential.

Figure 6-8 presents the optical microscope images of the thin films with a ratio MAPTMS/titanium butoxide 1/1, aged for 4h and cured at 60˚C labelled 1/1, 4(h), 60˚C a); 4/1 4(h), 60˚C b), 1/1 4(h) 80˚C c) 4/1,4(h), 80℃ as well as samples coated with 5 layers 1/1, 60˚C e) and 1/1, 80˚C f).
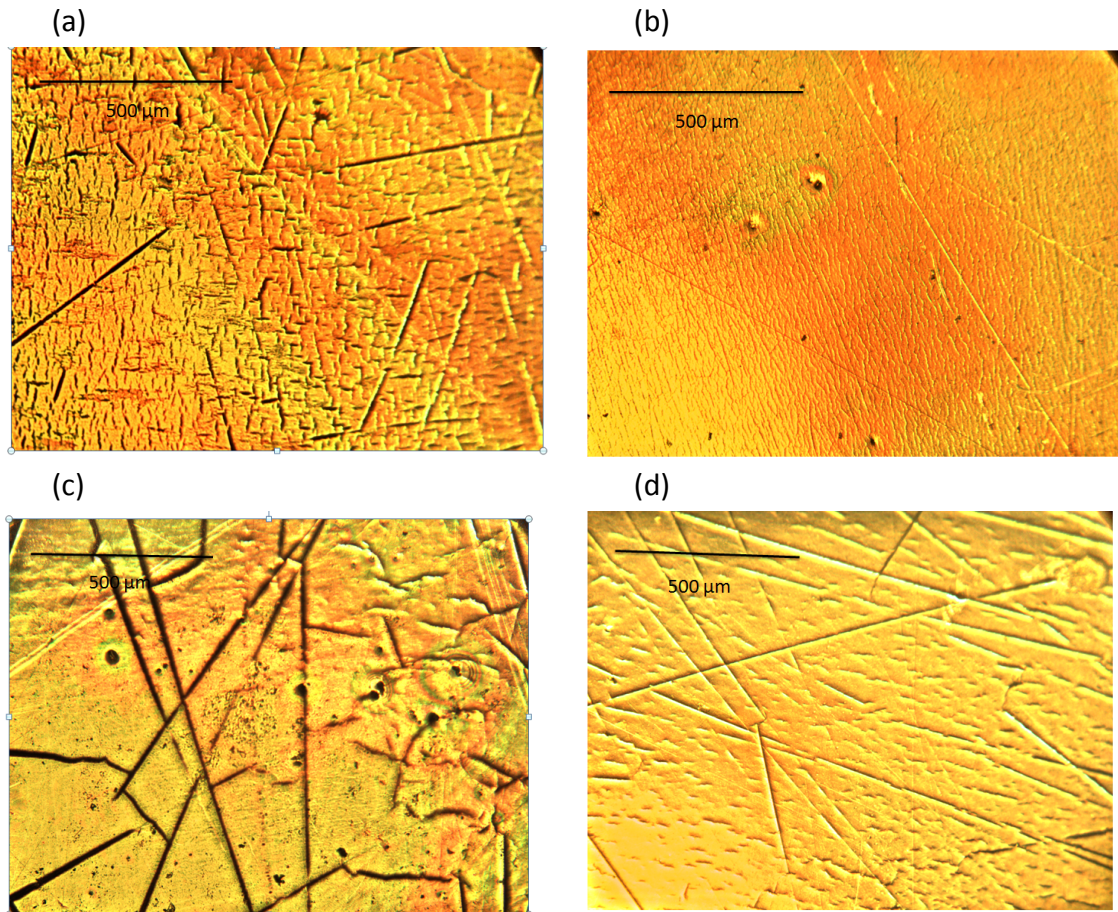
Figure 6-8 Optical image of 1/1,4(h),60˚C(a), 4/1,4(h),60˚C(b), 1/1,4(h),80˚C(c), 4/1,4(h),80˚C(d) perform (X5 magnification)

From Figure 6-8, large and deep cracks can be seen in samples with 1/1 while samples with 4/1 show a smoother surface with small cracks. The results from optical microscope are in agreement with AFM results, which show higher surface roughness for the samples with higher inorganic part.

The surface of hybrid sol-gel coating was observed by scanning electron microscopy. Figure 6-9 presents the morphology of the uncoated and coated substrate covered with sol 4/1, 4(h) and cured at 60 ˚C.
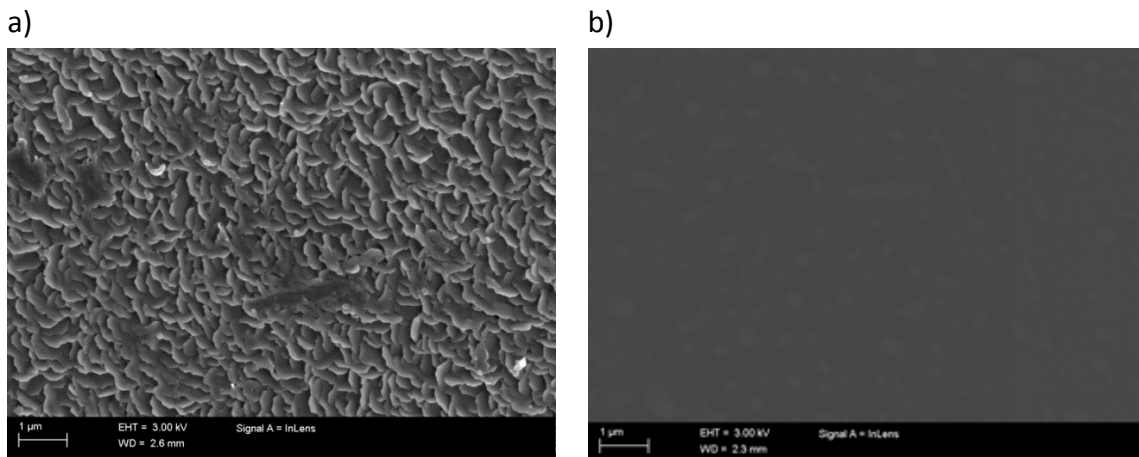
Figure 6-9 SEM picture ,surface morphology of uncoated sample(a) Coated sample with sol 4/1,4(h),60 ˚C(b)

As shown in Figure 6-9 (a) and (b), a significant change in surface morphology was found for the coated sample. Figure 6-9 (b) shows that the surface of magnesium has been fully covered by a uniform and crack free layer.

The EDS spectrum taken from area 1 is shown in Figure 6-10. From the Figure, presence of O, Si, Ti, Mg is revealed.

Element	O	Mg	Si	Ti	Total
Wt%	54	1	31	13	100
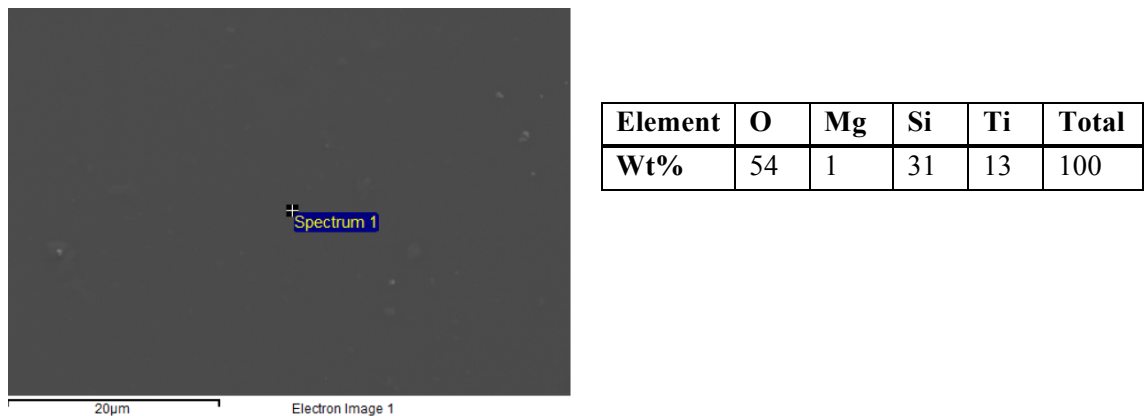
Figure 6-10 EDS spectrum of area 1

The average Rqs of the all surfaces related to five layer films are presented in Figure 6-11.
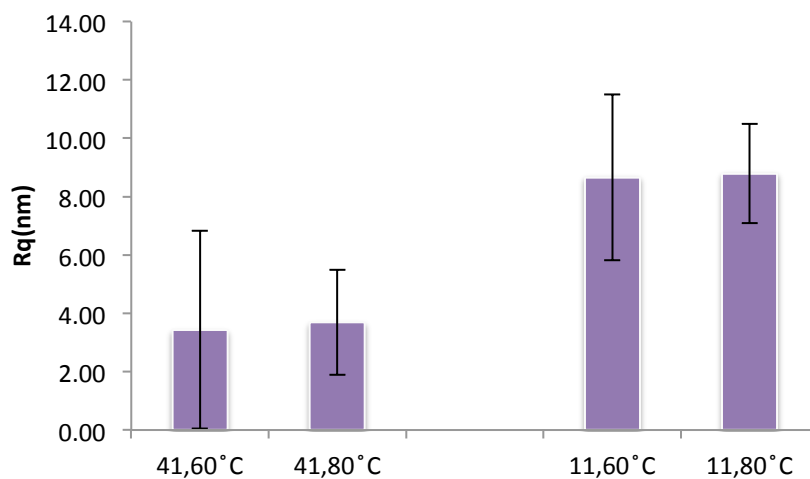
Figure 6-11 Average R_qS and their deviations of five layers film from Sol C at different MAPTMS/Titanum butoxide ratios and Temeratures. The data are averaged values from totally 4areas of 10 μm^2.

From Figure 6-11, a higher surface roughness can be noticed for samples with 1/1 ratio. The effect of the curing temperature on the surface roughness of samples coated with five layers is not significant, within the experimental accuracy of the measurements.

Figure 6-12 presents the optical microscope image of the thin films with a ratio MAPTMS/titanium butoxide 1/1, five layers which are cured at 80˚C labelled 1/1, 80˚C a); 4/1, 60˚C b).

(a)   (b)
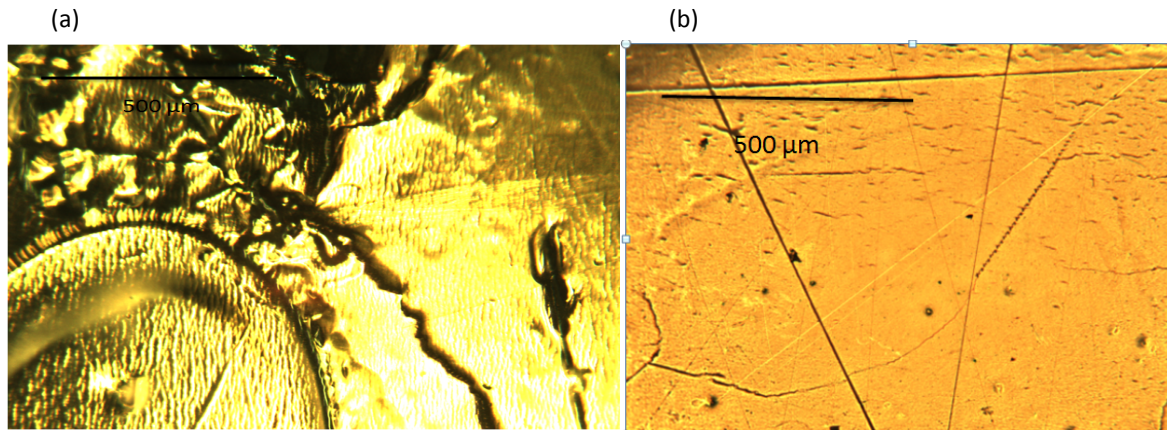
Figure 6-12 Optical image of 11,80˚C(a, 41,60˚C(b perform (X5 magnification)

As it can be understood from Figure 6-9, the results from optical microscope images are in agreement with results from AFM. The samples with 1/1 ratio show an agglomerated surface with deep cracks, which will result in a higher roughness.

It can be concluded that, increasing the organic components in sols will result in formation of denser films and reduces coating porosity. Furthermore, more flexible gel network will be formed that would be less prone to cracking during further drying process [6].

Figure 6-13 compares the surface roughness of samples, which are covered with one layer and five layers of film.
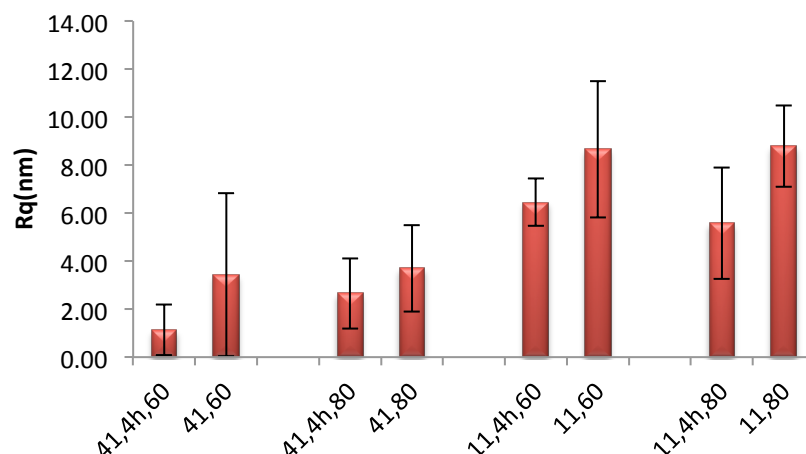
Figure 6-13 Comparison of average R_qs of one layer and five layers film from Sol C at different MAPTMS/titanum butoxide ratios and temeratures. The data are averaged values from totally 4areas of 10 μm^2

A higher surface roughness can be found for samples with five layers in comparison with samples that are coated with one layer.

During deposition, the film is heated at 60˚C and 80˚C during the night after each layer was applied. Curing the films at these temperatures will result in growth of grains.

So, the next applied layer will be deposited over films with established grain boundaries and cause bigger grains to be obtained. The results of the surface roughness indicate that, adjusting the number of layers deposited can control surface roughness. [77].

6.4.3 Contact angle

Wettability of the samples is a key factor, which is affecting the corrosion of implant in the body [78]. The surface wetting properties of the prepared hybrid films was characterised by contact angle measurement of ddH_2O by the sessile drop method. Figure 6-14 shows the photo images of water drops on the surface of sample which were covered by one layer of the thin films with a ratio MAPTMS/titanium butoxide 4/1, aged for 4h and cured at 60˚C labelled 4/1, 4(h), 60˚C a), 1/1 4h; 60˚C b), 4/1 24(h) 80˚C c) 1/1, 24(h), 80℃ d).

| (a) | (b) | (c) | (d) |
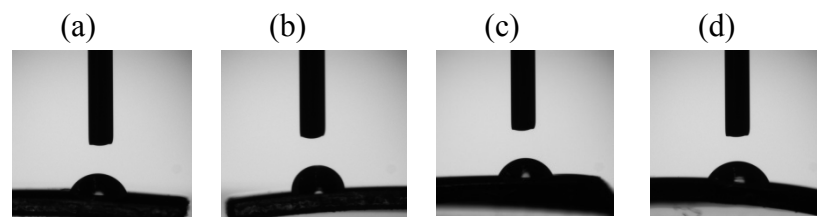
Figure 6-14 Photo images of water drops on the 4/1,4(h), 60˚C (a, 1/1,4(h),60˚C(b ,4/1,24(h), 80˚C(c, 1/1,24(h), 80 ˚C,d)

Figure 6-15 compares the effect of different ratios, curing temperature and aging time on water contact angle of one-layer hybrid films.
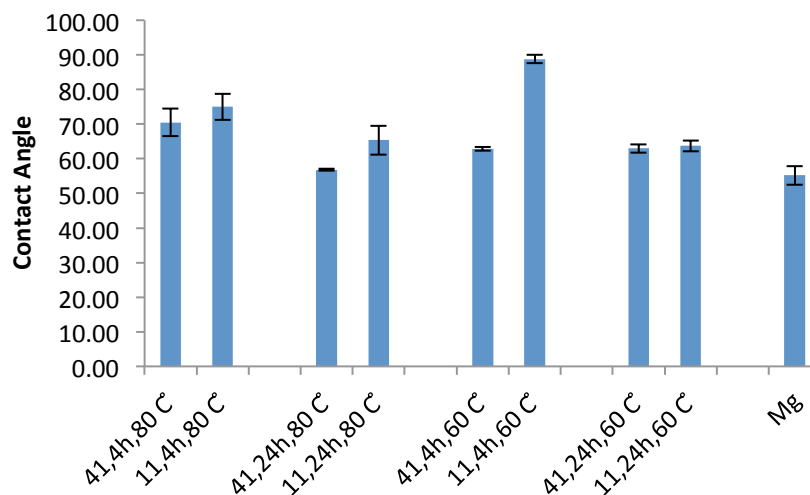
Figure 6-15 Effect of different ratios curing temperature and aging time on water contact angle

The contact angles of the coated substrates show values higher than that of the uncoated substrates indicating higher hydrophobicity. Contact angle recorded at the surface of the samples, which were coated with sol having ratio of 1/1, is higher than the samples, which were coated with sol having 4/1 ratio. These water contact angle values are consistent with the results obtained from roughness. It can be concluded that higher

surface roughness can increase the contact angle of surface remarkably and make the surface more hydrophobic [6].

Samples, which are aged for 4 hours, show a higher water contact angle rather than those, which were aged for 24 hours.

A higher water contact angle is characteristic of the more hydrophobic nature of the surface. Increased condensation of silanol groups, which causes denser reticulation, can increase the surface hydrophobicity [79]. In the case of samples with ratio of 4/1 which were aged for 4 hours and 1/1 which were aged for 24 hour, a higher hydrophilicity by increasing the curing temperature will be noticed which may result from the higher amount of TiOH groups remaining without reaction, probably due to insufficient curing temperature [80]. In this sense, the increase of water uptake into the hybrid coating can be responsible for the failure of the film upon immersion [81]. Samples 1/1, 4(h), 60℃ showed the highest water contact angles, indicating that the hybrid coatings are characterized by high cross-link density [81].

Figure 6-16 shows images of water drops on the surface of sample, which were covered by five layers (a) 4/1,80 ˚C (b) 4/1,60 ˚C (c) 1/1,80˚C (d) 1/1,60 ˚C.
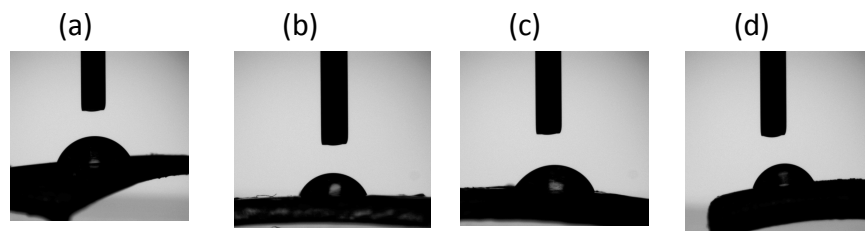
Figure 6-16 Photo images of water drops on the 5 Layer samples of 4/1,80˚C(a) 4/1,60˚C(b) 1/1,80 ˚C(c) 1/1,60˚C(d)

Figure 6-17 compares the effect of different ratios and curing temperature on water contact angle of five layer hybrid films.
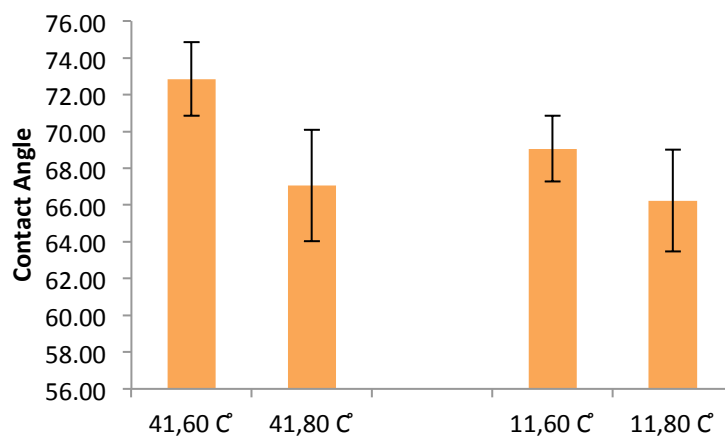
Figure 6-17 Effect of different ratios and curing temperature on water contact angle of five layer hybrid films

From the Figure, it can be understood that the samples that are cured at 60℃ show a higher water contact angle in comparison with the ones, which have been cure at 80 ˚C. This can be related to the higher water content in samples which are cured at 60 ˚C The

highest water contact angle is related to the sample with 4/1 ratio (Θ=72.85±2.01) which has been cured at 60˚C.

Figure 6-18 presents a comparison of water contact angle of samples that are covered by one and five layer.
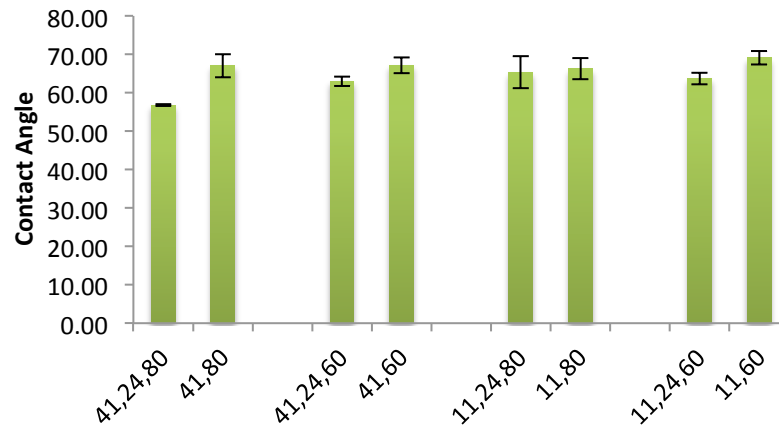
Figure 6-18 Comparison of water contact layer of one layer and five layer samples

As it can be understood the samples with five layers show a higher water contact angle. This can be related to a higher surface roughness or higher water content in samples with five layers.

6.4.4 Attenuated total reflectance-Fourier transform infrared (ATR-FTIR) measurements

The chemical structure of the modified sol C was studied by ATR-FTIR. Figure 6-19 presents the ATR-FTIR spectra of the coatings with a ratio 1/1, cured at 60˚C and aged for 4h and 24h. The spectra were background corrected and normalised to the band with maximum intensity. The main absorption bands and their attributions are listed in Table 6-4.
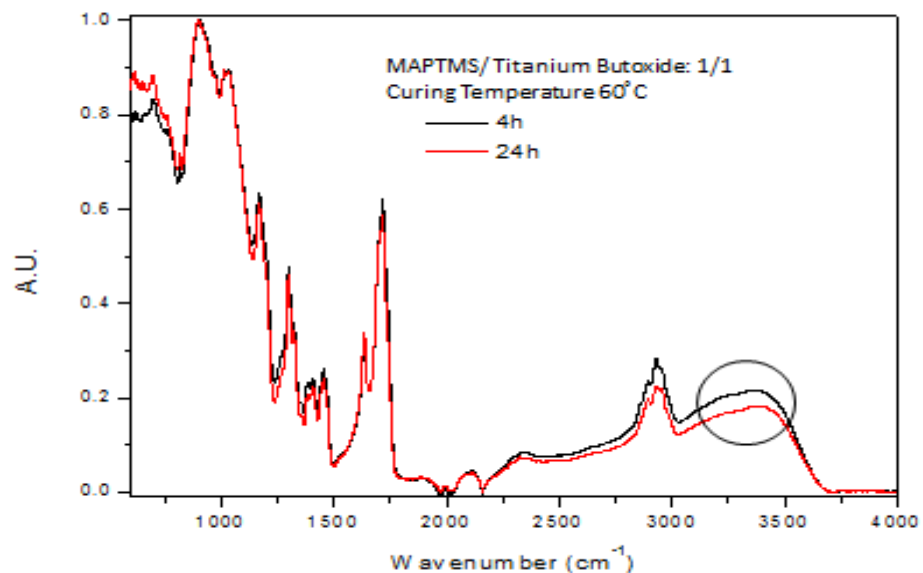
Figure 6-19 ATR-FTIR spectra of Sol 1/1 cured at 60˚C ,Aging time 4(h)and 24(h)

Table 6-4 The ATR-FTIR absorption bands of modified sol C

Wavelength Cm^{-1}	Bands	Reference
3200-3600	O-H	[82]
2900-3200	C-H (alkyl)	[83]
2840	C-H (Methoxy)	[83]
1720	C=O (MAPTMS)	[83]
1640	C=C (MAPTMS)	[83]
1410-1450	C–H (CH_2 and CH_3)	[83]
	C-O stretching	[84]
1300-1320	Asymmetric stretching vibrations of C-O of C-O-C	[83]
1000-1130	Si-O-Si	[85]
		[86]
900- 1000	Si-O-Metal	[86]
1090	C-C-O for pure ethanol	[83]
1030	Si-O stretching	[84]
	Si-O-Si stretching	
1015	Si-O-Si	[85]
980	Si-O-Si	[83]
950–1200	Mg-O-Si	[87]
925	Ti-O-Si	[86]
910	Ti-O-Si	[88]
900	Si-OH	[89]
800–820	Symmetric stretching vibrations of Si-O-Si and Si-O	[85]
		[90]
780	Si-C	
655	Ti-O-Ti	[91]

The absorption band at 3200-3500cm^{-1} is related to OH group. The absorption bands around 2950 and 2840 cm^{-1} are attributed to stretching vibrations of C-H bonds in alkyl and methoxy groups, respectively [83]. The band close to 1720 cm^{-1} is associated to the stretching vibrations of C=O carbonyl groups of MAPTMS, while the one at 1640 cm^{-1} is attributed to C=C groups of the methacrylate groups from the MAPTMS precursors [83]. The bands at 1450 cm^{-1} can be attributed to deformation vibrations of C–H in CH_2 and CH_3 bonds. The asymmetric and symmetric stretching vibrations of C-O of C-O-C bonds are centered at 1320 and 1300 cm^{-1}, respectively [83].

All the bands are characteristic of thin films obtained from MAPTMS and titanium butoxide precursors. In Figure 6-19, one can see that the only major differences lie in the high wavenumber region. This region corresponds to the molecular and adsorbed water in the coating structure. With an increase in the aging time a decrease in the OH band is seen. This is in agreement with the lower water contact angle obtained for the materials aged for longer time. Absence of asymmetric stretching vibration of the Si-O-

C and Ti-O-C, which appears at 1080 cm^{-1} implies the end of the hydrolysis process in the sol-gel [92, 83].

Figure 6-20 presents the sample with ratio 1/1 cure at various temperatures a) and having 1 or 5 layers b).

(a)
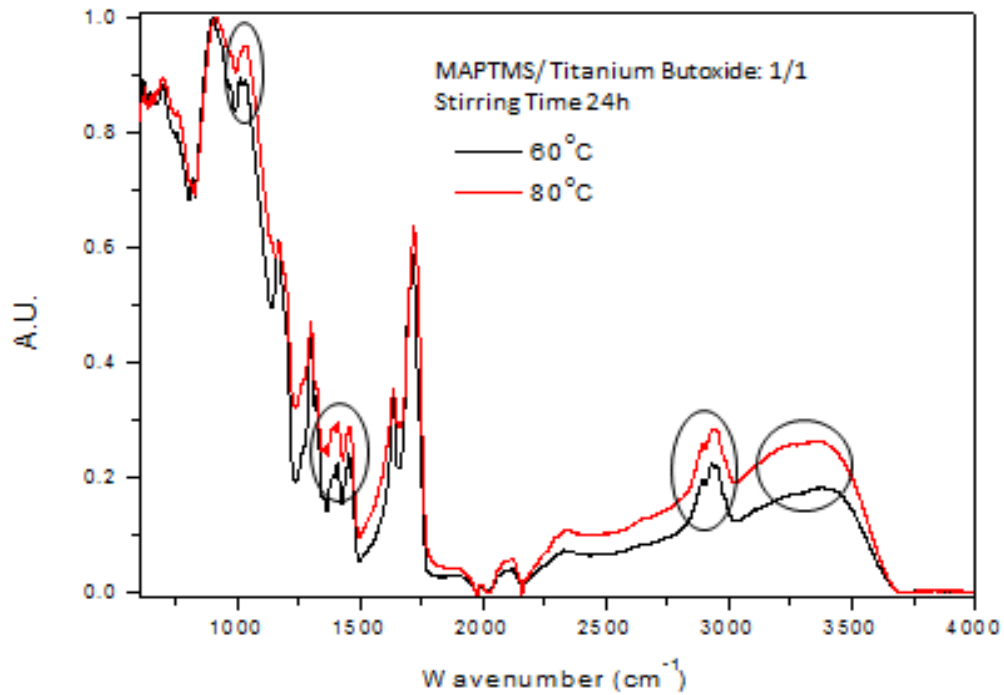
(b)
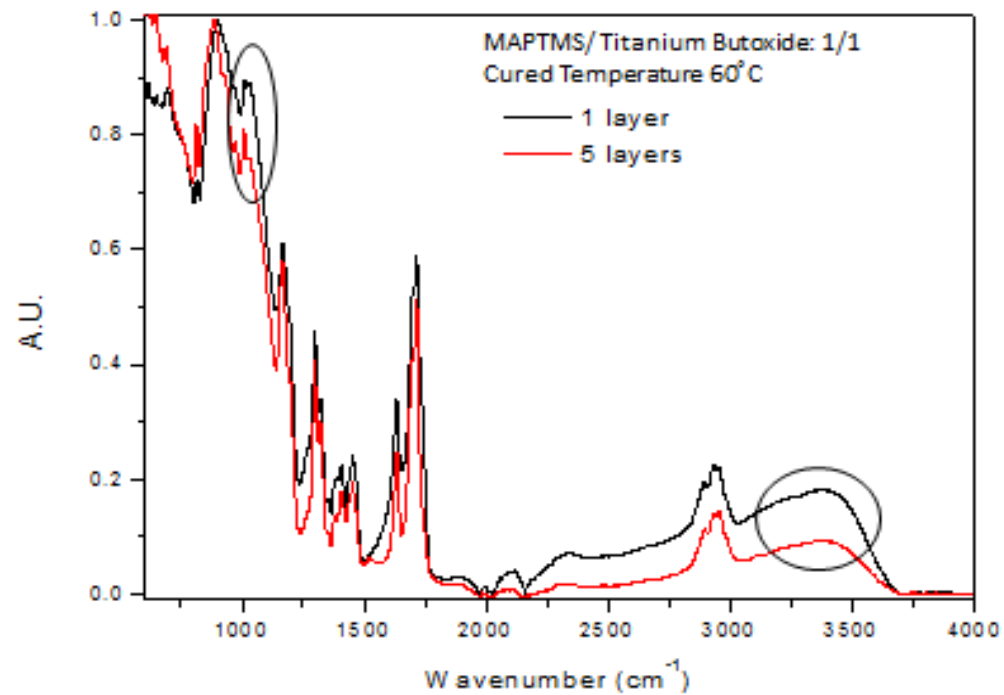
Figure 6-20 ATR-FTIR spectra of sample with ratio 1/1 cure at various temperatures a) and having 1 or 5 layers b)

The intensity of absorption peaks of the samples, which were cured at 60°C, is lower at wavenumbers of 3380cm^{-1}, which indicates, lower amount of water. This is in agreement with lower water contact angle for these samples (64°±1.5) in comparison with the ones which were cured at 80°C (65° ± 4.2). Weaker peaks between 1000-1030 cm^{-1} and 910-925 cm^{-1} show that lower Si-O-Si and Ti-O-Si bands has been formed in this samples indication of a more cross-linked structure consisting of polysiloxanes.

Figure 6-21 shows the respective ATR-FTIR spectra of Sol 4/1, cured at 60°C, aging time 4(h) and 24(h).
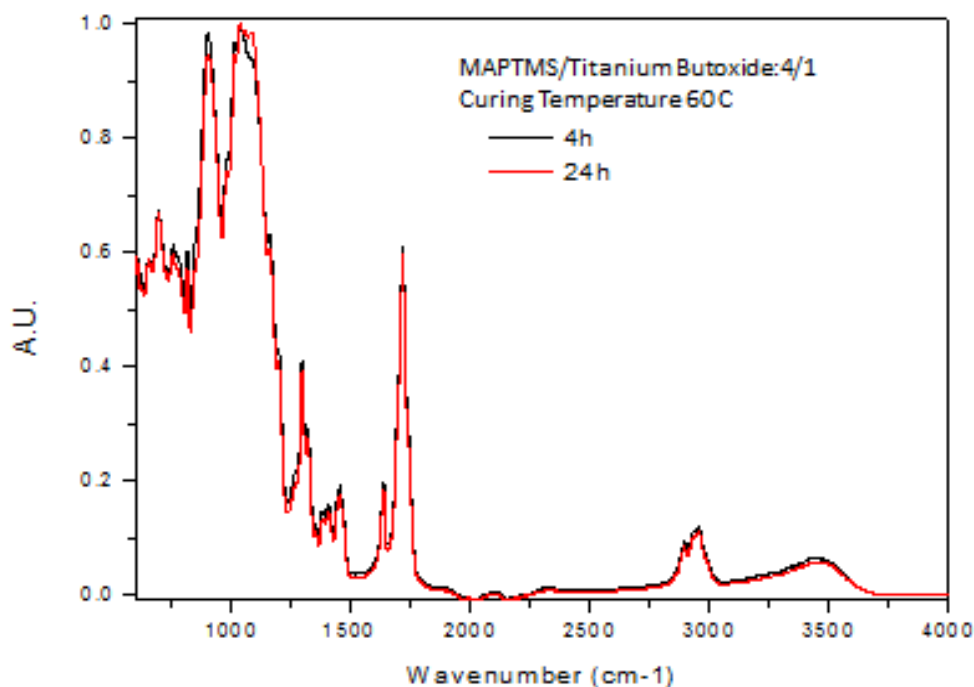
Figure 6-21 ATR-FTIR spectra of Sol 4/1, cured at 60°C, Aging time 4(h) and 24(h)

As it can be understood all the absorption peaks are overlapping which indicates that the aging time does not affect the chemical structure of the sol. As it was mentioned before, wavenumber between 1000-1130cm^{-1} is related to Si-O-Si peaks. The absorption peak is broader in case of samples, which are aged for 24 (h), which indicate that Si-O-Si bands have become longer and branched [86]. Absence of asymmetric stretching vibration of the Si-O-C and Ti-O-C, which appears at 1080 cm^{-1} implies that the hydrolysis process was complete already after 4h of aging [92].

Figure 6-22 shows the respective ATR-FTIR spectra of Sol 4/1, aged 4(h), cured at 60°C and 80°C. From Figure 6-22, it can be understood that curing the samples even at 60 or 80°C does not affect the chemical structure of sol C with MAPTMS/titanium butoxide: 4/1 [83].
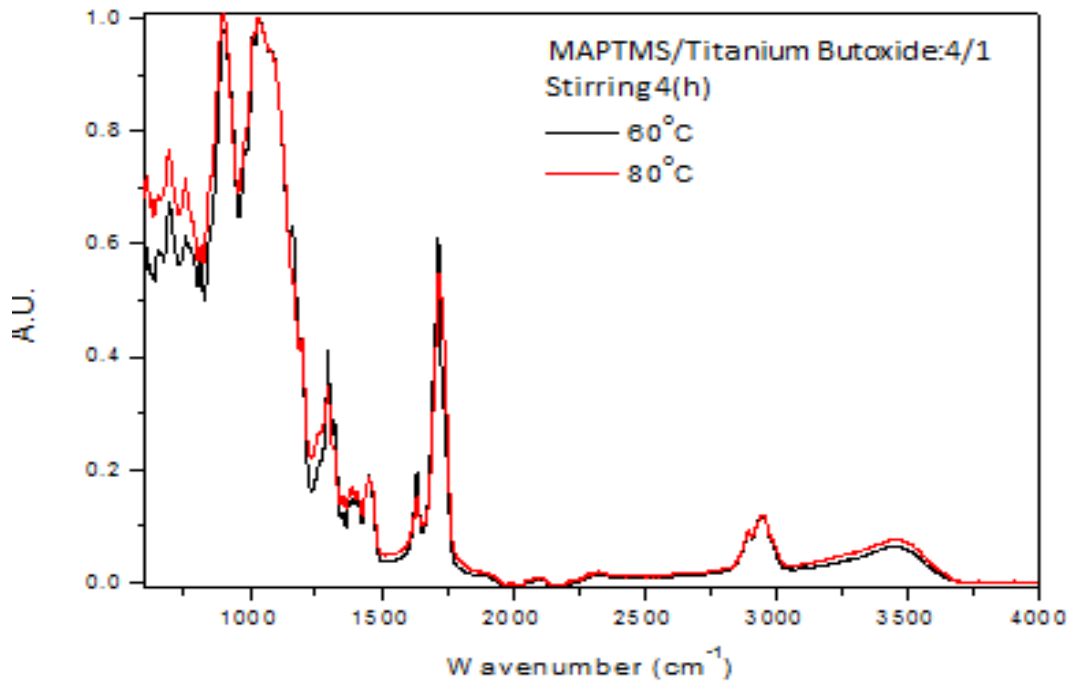
Figure 6-22 ATR-FTIR spectra of Sol 4/1, aged 4(h), cured at 60°C and 80°

Figure 6-23 compares the effect of number of layers on the chemical structure of film with 4/1 ratio which were cured at 60°C.
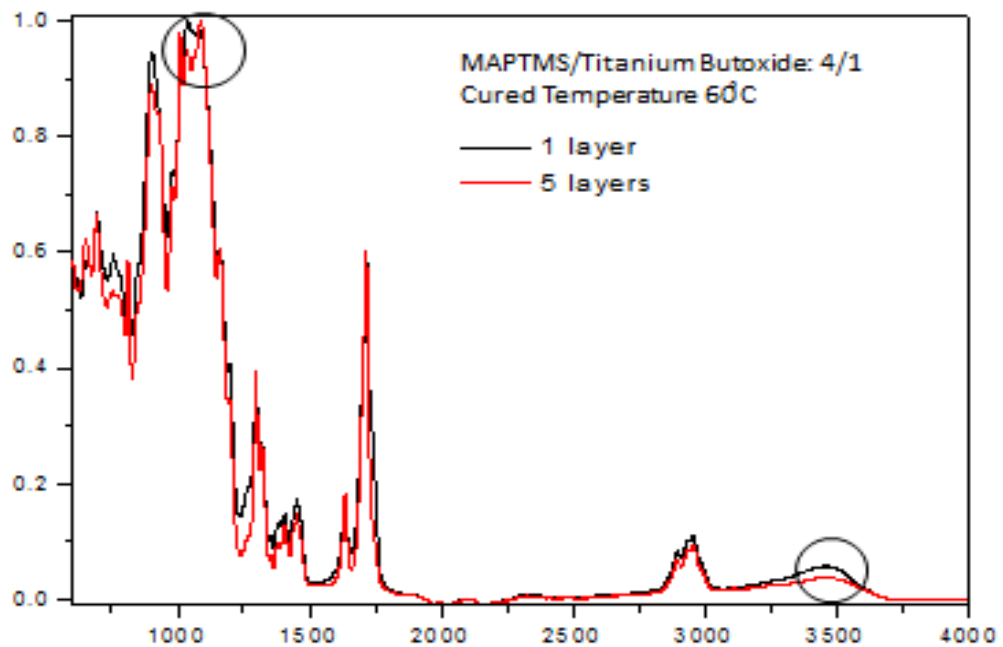
Figure 6-23 effect of number of layers on the chemical structure of film which were cured at 60° C

Lower intensity at peaks 3380 cm^{-1} indicates lower amount of water in films with five layers. This is in contrast with results obtained from water contact experiment, since the samples with five layers show a higher water contact angle. This difference in results can be related to a higher roughness in samples with five layers, which can cause an increase in water contact angle. The peaks at wavelength between 1000-1080 cm^{-1} are

broader in case of samples with five layers, which indicates that Si-O-Si bands have become longer and branched [86].

Figure 6-24 presents the ATR-FTIR spectra of the samples coated with five layers of sol with ratio 1/1 and 4/1.
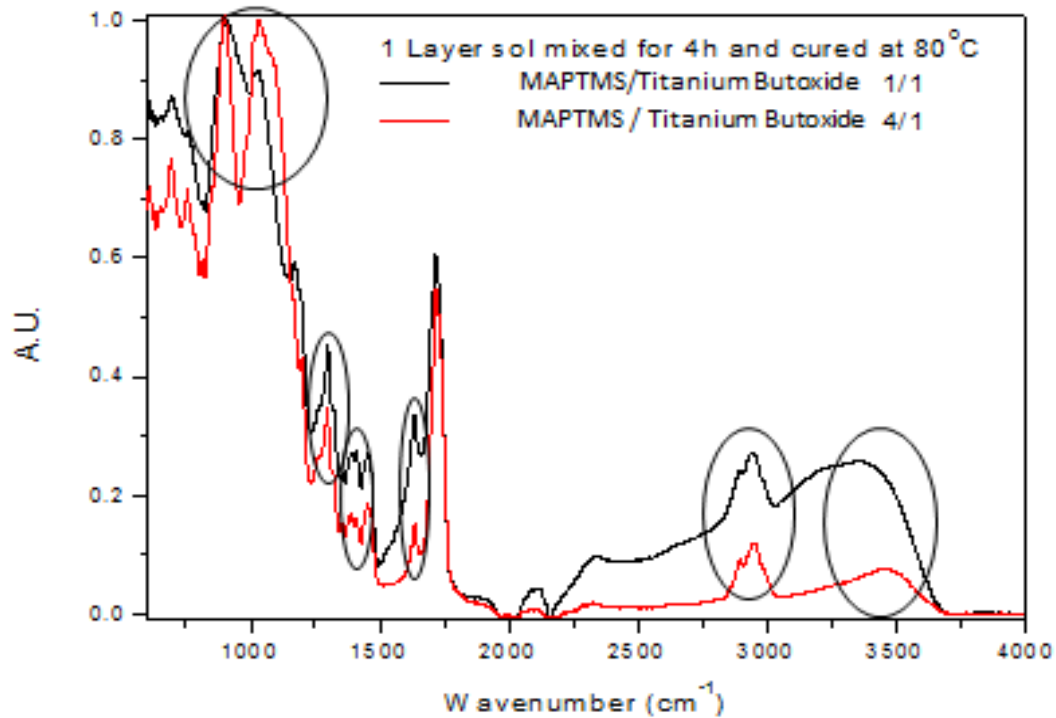
Figure 6-24 ATR-FTIR absorption spectra of MAPTMS/TMOS:Black(1/1),Red(4/1)

From Figure 6-24 one can see that a 1/1 ratio leads to an OH band with higher intensity. This is in agreement with the higher contact angle recorded for this sample. Further an increase in the MAPTMS leads to higher content of Si-O-Si bonds as seen with the increase in the band at1000-1130 cm^{-1} and a higher concentration of C-O and C-H vibration as can be seen with the increased intensity of the bands in the 1200-1750 cm^{-1} region. A similar discussion can be made for the samples coated with five layers of the sol with ratios 1/1 and 4/1 cured at 80˚C.

6.4.5 Immersion test

Immersion tests were also performed to evaluate the various coatings capability to enhance the substrate corrosion resistance. Before immersion in SBF, the uncoated magnesium side of substrate presents a bright silver surface, but the surface of the coated sample exhibit a uniform and yellowish appearance due to presence of the coating. In order to compare the corrosion morphology of the substrate, uncoated and coated samples were soaked in SBF for 6, 24 and 72 hours.

Table 6-5 shows photographs of the coated samples as a function of coating type and immersion times.

Table 6-5 Corrosion morphology of the coated samples after the immersion in SBF for different period
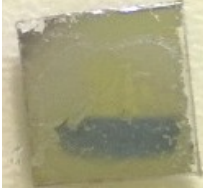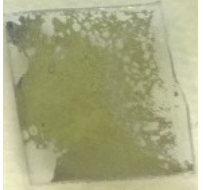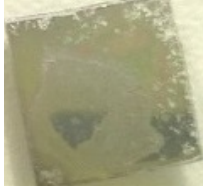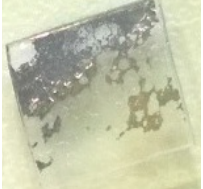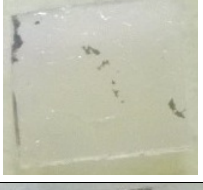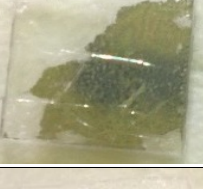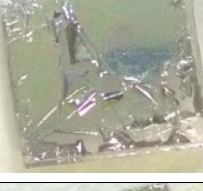
Sample	6(h)	24(h)	72(h)
4/1,4h, 60˚C			
4/1,24h, 60˚C			
4/1,4h, 80˚C			
4/1,24h, 80˚C			
1/1,4h, 60˚C			
1/1,24h, 60˚C			
1/1,4h, 80˚C			
1/1,24h, 80˚C			

Table 6-6 shows photographs of the uncoated samples as a function of coating type and immersion times.

Table 6-6 Corrosion morphology of the uncoated samples after the immersion in SBF for different period

	6(h)	24(h)	72(h)
Uncoated			
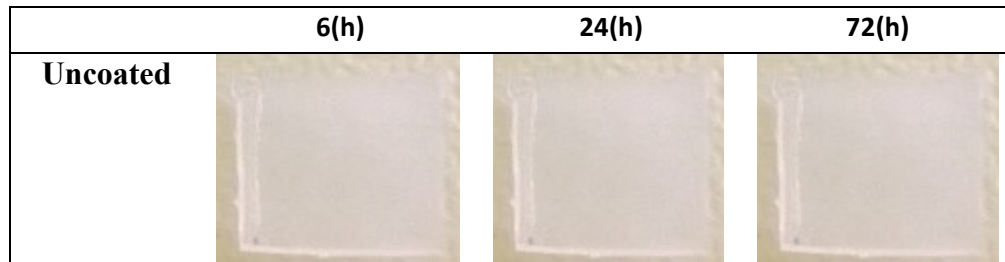
As it can be understood from Table 6-6, after few minutes of immersion, the magnesium layer on the uncoated samples starts to react with water and is removed completely. Although the coated samples suffered from minor corrosion after 6 hours of immersion, most of the surfaces still displayed silver metallic luster. This means that the film protects the magnesium layer for few hours. The best corrosion resistance behavior can be seen in sol 4/1,4h, 60°C, 4/1,24h, 60°C, 1/1,4h, 60°C and 1/1,24h, 60°C. Herein, it could inferred that curing the samples at 80°C has caused surface defects such as appearance of small cracks which led to the SBF to penetrate the film. This is in agreement with results, which were obtained from optical microscope images. The coating may have been damaged due to the excessive deformation of substrate as a result of difference in modulus and thermal expansion coefficient of the coating and substrate [41].

As SBF penetrates through the film, the magnesium layer starts to react which will result in hydrogen production [2]. Pressure of produced hydrogen can play a destructive role and result in opening up the film. This can reduce the effectiveness of the film.
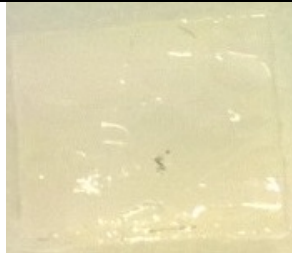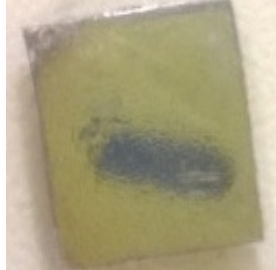
It seems that samples with MAPTMS/titanium butoxide: 4/1, which were aged for four hours and cured at 60℃, was the best protective coating even after 24 hours. As it can be seen the corrosion was detected only at the edges of the sample. None of the samples were capable to preserve their protective role at 72 hours of immersion.

In order to prevent the SBF from diffusing through the film, five layers of films were applied on the substrate. The effect of number of layers, on corrosion resistance behavior of the films after immersion has been illustrated in Table 6-7.

Similar to the film with one layer, the best protection can be noticed for the films, which have been cured at 60℃ due to lower surface defects. As it can be seen, sample with MAPTMS/titanium butoxide: 1/1 that has been cured at 60℃ could protect the magnesium layer only for 6 hours. The surface of this sample is bended which may cause defects on the surface or detachment of film to the surface. Sample with MAPTMS/titanium butoxide 4/1 shows a good protection even after 72 hours by showing a silver metallic luster surface. As it can be seen the magnesium has been removed from the edges of the sample. This can be related to the slight degradation of hybrid film that will result in appearance of small cracks on the edge [93]. Investigating the

samples after 72 hours indicates that, although the magnesium layer has been removed in most of the cases in some cases the magnesium coating was not fully removed.

Table 6-7 Corrosion morphology of the uncoated and coated samples with five layer of films after the immersion in SBF for different period

	6(h)	24(h)	72(h)
41,80			
41,60			
11,80			
11,60			
Uncoated			

7 CONCLUSION

The aim of this study was to define a sol-gel recipe that can be densified at low temperatures while being biocompatible in order to prepare a fully biodegradable and biocompatible resonant sensor. The resonant sensor is composed an Mg layer deposited onto a PLA sheet. Uniform TiO_2 thin films were successfully prepared on polymeric substrates, using a sol-gel method and dip-coating technique. Absorbed laser radiation with wavelength of 1.06 nm was used for densification of inorganic films. It was found that despite changing the irradiation parameters the beam heated the Mg layer and caused damage. This is due to the fact that titanium dioxide sol-gel is transmitting the radiation at this wavelength. The radiation is absorbed by the metallic layer and causes an increase in temperature, which will result in melting of the substrate. Since titania films absorb the radiation in the UV and IR spectral region, excimer lasers or CO_2 lasers are suggested to be used for densification of films. In case of using lasers emitting in the NIR region, an adsorbing metal claddings should be used to prevent transition of laser radiation through the film.

Hybrid sol was synthesized using a sol-gel process based on MAPTMS and TMOS. The films were deposited using dip coating. Due to the difference in modulus and thermal expansion coefficient between the polymer substrate and the hybrid coating, the substrate was extensively bended which caused the magnesium layer and applied film to be damaged and removed.

Hybrid coating based on MAPTMS and titanium butoxide was prepared on polymeric substrates by using the sol-gel method and dip-coating technique. Within this sol-gel several parameters such as organic/inorganic ratio, aging time, curing temperature and number of applied layers were changed to enhance the corrosion resistance of the coating.

Low contact angle of modified sols on the substrate indicated a high wettability of different sols showing that the sol should cover and bond nicely to the substrate. Upon film deposition, the results from AFM pictures, optical microscope, water contact angle and FTIR show a higher roughness, surface cracks, hydrophobicity and water content for coatings with a higher inorganic component. It was found that changes in surface roughness influence the wetting characteristics of the thin films. An increase in surface roughness was found to increase the water contact angle significantly, thereby decreasing the wettability of the thin films.

It was found that inorganic content has a significant effect on corrosion properties of sol–gel coatings. Coatings at higher inorganic content had higher porosity due to formation of larger linear titania chains and stronger gel network. This will result in pres-

ence of microcracks, which are pathways for the corrosive environments to reach the magnesium layer, and are the origin of deterioration of the coatings. As a result, a decrease in corrosion protection properties of such coatings is noticed. Furthermore, the risk of fracture will be increased in sol-gels with higher inorganic content. This is due to the stress, which is concentrated at sintered necks between particles.

The SEM pictures from the surface of the sample, which is covered by a film, indicates formation of a uniform and crack free layer, which can cause significant change in surface morphology of substrate. The results from AFM pictures and optical microscope show that the effect of aging time on the surface roughness is insignificant. By comparing the surface roughness, it can be concluded that 4/1 samples which are cured at 60 ˚C and 1/1 samples, which are cured at 80˚C, show a lower porosity and crack forming potential. A higher surface roughness and water contact angle for samples, which are covered with five layers in comparison with the ones with one layer, was noticed. ATR-FTIR spectra of the samples indicate higher water content for samples with one layer.

It was concluded that the most promising samples were the ones containing lower inorganic content, which were cured at 60˚C and coated with five layers.

As the future goals, particles can be added to the hybrid sol to increase film thickness and to prevent the cracking. The hybrid coating can be doped with slow release of corrosion inhibitors, which can provide a long-term anticorrosion behaviour for substrate.

8 BIBLIOGRAPHY

[1] T. Salpavaara, V. Ellä , M. Kellomäki, and J. Lekkala, "Biodegradable passive resonance sensor- fabrication and initial testing," in *International conference on biomedical electronics and devices*, Lisbon, 2015.

[2] N. T. Kirkland, N. Birbilis, and M. P. Staiger, "Assessing the corrosion of biodegradable magnesium implants: a critical review of current methodologies and their limitations," *Acta biomaterialia,* vol. 8, no. 3, pp. 925-936, 2012.

[3] L. I. U. Jingxiao, S. H. I. Fei, and Y. A. N. G. Dazhi, "Characterization of sol-gel-derived TiO_2 and TiO_2-SiO_2 films for biomedical applications," *Materials science & technology,* vol. 20, no. 5, pp. 550-554, 2004.

[4] L. L. Hench, and J. K. West, "The sol-gel process," *Chemical Reviews,* vol. 90, no. 1, pp. 33-72, 1990.

[5] T. M. Harrell, B. Hosticka, M. E. Power, L. Cemke, R. Hull, and P.M. Norris, "Selective deposition of biocompatible sol-gel materials," *Sol-gel science and technology,* vol. 31, no. (1-3), pp. 349-352, 2004.

[6] S. Zheng, and J. Li, "Inorganic–organic sol-gel hybrid coatings for corrosion protection of metals," *Sol-gel science and technology,* vol. 54, no. 2, pp. 174-187, 2010.

[7] L. Filipovic, S. Selberherr, G. C. Mutinati, E. Brunet, S. Steinhauer, A. Köck, and F. Schrank, "Modeling spray pyrolysis deposition," *Proceedings of the world congress on engineering,* vol. 2, pp. 987-992, 2013.

[8] C. Höglund, "Reactive magnetron sputter deposition and characterization of thin films from the Ti-Al-N and Sc-Al-N systems," 2009.

[9] E. Morintale, C. Constantinescu, and M. Dinescu, "Thin films development by pulsed laser-assisted deposition," *Annals of the University of Craiova Physics AUC,* vol. 20, pp. 43-56, 2010.

[10] T. Nakamura, E. Matsubara,N. Sato,A. Muramatsu, and H. Takahashi, "Study on fabrication of titanium oxide films by oxygen pressure controlled pulsed laser deposition," *Materials transactions,* vol. 45, no. 7, pp. 2068-2072, 2004.

[11] Q. Bao, C. Chen, D. Wang, Q. Ji, and T. Lei, "Pulsed laser deposition and its current research status in preparing hydroxyapatite thin films," *Applied Surface Science,* vol. 252, no. 5, pp. 1538-1544, 2005.

[12] S. M. Kaczmarek, "Pulsed laser deposition—today and tomorrow," *Laser*

technology V: applications in materials sciences and engineering, vol. 3187, pp. 129-134, 1997.

[13] V. Barranco, N. Carmona, J. C. Galván, M. Grobelny, L. Kwiatkowski, and M. A. Villegas, "Electrochemical study of tailored sol–gel thin films as pre-treatment prior to organic coating for AZ91 magnesium alloy," *Progress in Organic Coatings,* vol. 68, no. 4, pp. 347-355, 2010.

[14] R. Eason, Pulsed laser deposition of thin films: applications-led growth of functional materials, John Wiley & Sons, 2007.

[15] E. Alfonso, J. Olaya, and G. Cubillos, "Thin film growth through sputtering technique and its applications," in *Crystallization–Science and Technology*, 2012, pp. 397-432.

[16] K. A. Walsh, Beryllium chemistry and processing, ASM International, 2009.

[17] D. Yang, Nanocomposite films for gas sensing, INTECH Open Access Publisher, 2011, pp. 857-882.

[18] K. L. Choy, "Chemical vapour deposition of coatings," *Progress in materials science,* vol. 48, no. 2, pp. 57-170, 2003.

[19] H. O. Pierson, Handbook of chemical vapor deposition: principles, technology and applications, William Andrew, 1999.

[20] D. Perednis, and L. J. Gauckler, "Thin film deposition using spray pyrolysis," *Electroceramics,* vol. 14, no. 2, pp. 103-111, 2005.

[21] A. Purwanto, W. N. Wang, K. Okuyama, "Flame Spray Pyrolysis," in *Handbook of Atomization and Sprays*, Springer US, 2011, pp. 869-879.

[22] T. Karhunen, A. Lähde, J. Leskinen, R. Büchel, O. Waser, U. Tapper, &and J. Jokiniemi, "Transition metal-doped lithium titanium oxide nanoparticles made using flame spray pyrolysis," *International scholarly research network,* vol. 2011, pp. 1-6, 2011.

[23] J. R. Davis, Handbook of thermal spray technology, ASM international., 2004.

[24] D. O. V. Uche, "Sol-gel technique: A veritable tool for crystal growth," *Advances in applied science research,* vol. 4, no. 1, pp. 506-510, 2013.

[25] M. Jokinen, E. Györvary, and J. B. Rosenholm, "Viscoelastic characterization of three different sol–gel derived silica gels," *Colloids and surfaces A: Physicochemical and engineering aspects,* vol. 141, no. 2, pp. 205-216, 1998.

[26] A. Duran, Y. Castro, M. Aparicio, A. Conde, and J. J. de Damborenea, "Protection and surface modification of metals with sol–gel coatings," *International materials reviews,* vol. 52, no. 3, pp. 175-192, 2007.

[27] M. N. Rahaman, Ceramic processing, John Wiley & Sons, Inc, 2006.

[28] C. J. Brinker, and G. W. Scherer, Sol-gel science: the physics and chemistry of sol-gel processing, Gulf Professional Publishing, 1990.

[29] H. M. Nur, "Fabrication of advanced ceramics and selective metallization of non-

conductive substrates by inkjet printing," Brunel University, 2002.

[30] M. Jokinen, Bioceramics by sol-gel method : processing and properties of monoliths, films and fibres, Åbo Akademi University, Department of Physical Chemistry, 1999.

[31] J. Shi, Steric Stabilization, Ohio, 2002.

[32] C. A. Milea, C. Bogatu, and A. Duţă, "The influence of parameters in silica sol-gel process.," *Bull Trans Univer Braşov Ser I Eng Sci,* vol. 4, pp. 59-66, 2011.

[33] G. Kickelbick, "Hybrid Materials–Past, Present and Future," *Hybrid Materials,* vol. 1, no. 1, pp. 39-51, 2014.

[34] J. Wen, and G. L. Wilkes, "Organic/inorganic hybrid network materials by the sol-gel approach," *Chemistry of Materials,* vol. 8, no. 8, pp. 1667-1681, 1996.

[35] R. B. Figueira, C. J. R. Silva, and E.V. Pereira, "Organic–inorganic hybrid sol–gel coatings for metal corrosion protection: a review of recent progress," *Coatings Technology and Research,* vol. 12, no. 1, pp. 1-35, 2014.

[36] C. McDonagh, F. Sheridan, T. Butler, and B. D. MacCraith, "Characterisation of sol-gel-derived silica films," *Non-crystalline solids,* vol. 194, no. 1, pp. 72-77, 1996.

[37] Y. F. Joya, "Titanium Dioxide Films Prepared by Sol-Gel/Laser-Induced Technique for Inactivation of Bacteria," 2011.

[38] F. Sayilkan, M. ASİLTÜRK, H. Sayilkan, Y. Önal, M. Akarsu, and E.Arpaç, "Characterization of TiO_2 Synthesized in Alcohol by a Sol-Gel Process: The Effects of Annealing Temperature and Acid Catalyst," *Turkish Journal of Chemistry,* vol. 29, no. 6, pp. 697-706, 2006.

[39] M. A. Fardad, "Catalysts and the structure of SiO_2 sol-gel films," *Materials science,* vol. 35, no. 7, pp. 1835-1841, 2000.

[40] S. M. Attia, "Nanostructure study of Tio2 films prepared by dip coating process," vol. 18, no. 1, 2002.

[41] J. D. Mackenzie, and E. Bescher, "Some factors governing the coating of organic polymers by sol-gel derived hybrid materials," *Sol-gel science and technology,* vol. 27, no. 1, pp. 7-14, 2003.

[42] S. M. Attia, "Review on Sol-Gel Derived Coatings: Process, Techniques and Optical Applications.," *Material science and technology,* vol. 18, no. 3, pp. 211-218, 2002.

[43] J. Pütz, G. Gasparro, and M. A. Aegerter, "Liquid film spray deposition of transparent conducting oxide coatings," *Thin solid films,* vol. 442, no. 1, pp. 40-43, 2003.

[44] L. Besra, and M. Liu, "A review on fundamentals and applications of electrophoretic deposition (EPD).," *Progress in materials science,,* vol. 52, no. 1, pp. 1-61, 2007.

[45] D. J. Taylor, J. P. Cronin, L. F. Allard, and D. P. Birnie, "Microstructure of laser-fired, sol-gel-derived tungsten oxide films," *Chemistry of materials,* vol. 8, no. 7, pp. 1396-1401, 1996.

[46] J. L. Keddie, P. V. Braun, and E. P. Giannelis, "Interrelationship between densification, crystallization, and chemical evolution in sol-gel titania thin films," *American Ceramic Society,* vol. 77, no. 6, pp. 1592-1596, 1994.

[47] R. A. Antunes, M. C. L. de Oliveira, and M. F. Pillis, "Effect of the deposition temperature on the corrosion stability of TiO_2 films prepared by metal organic chemical vapor deposition," *International Journal of Electrochemical Science,* vol. 8, pp. 1487-1500, 2013.

[48] J. X. Liu, F. Shi, and D. Z. Yang, "Characterization of sol-gel-derived TiO_2 and TiO_2-SiO_2 films for biomedical applications," *Materials science and technology,* vol. 20, no. 5, pp. 550-554, 2004.

[49] N. Moritz, M. Jokinen, T. Peltola, S. Areva, and A. Yli-Urpo, "Local induction of calcium phosphate formation on TiO_2 coatings on titanium via surface treatment with a CO_2 laser.," *Biomedical materials research Part A,* vol. 65, no. 1, pp. 9-16, 2003.

[50] X. Y. Tao, I. Fsaifes, V. Koncar, C. Dufour, C. Lepers, L. Hay, L., and M.Bouazaoui, "CO_2 laser-induced crystallization of sol–gel-derived indium tin oxide films," *Applied physics A,* vol. 96, no. 3, pp. 741-749, 2009.

[51] L. C. Klein, Sol-gel optics: processing and applications, Springer, 1994.

[52] N. Moritz, S. Areva, J. Wolke, and T. Peltola, "TF-XRD examination of surface-reactive TiO_2 coatings produced by heat treatment and CO_2 laser treatment," *Biomaterials,* vol. 26, no. 21, pp. 4460-4467, 2005.

[53] K. Starbova, V. Yordanova, D. Nihtianova, W. Hintz, J. Tomas, , and N. Starbova, "Excimer laser processing as a tool for photocatalytic design of sol–gel TiO_2 thin films," *Applied surface science,* vol. 254, no. 13, pp. 4044-4051, 2008.

[54] N. Asakum, T. Fukui, M. Aizawa, M. Toki, H. Imai, and H. Hirashima, "Ultraviolet-laser-induced crystallization of sol-gel derived inorganic oxide films," *Sol-gel science and technology,* vol. 19, no. 1-3, pp. 333-336, 2000.

[55] H. Imai, K. Awazu, M. Yasumori, H. Onuki, and H. Hirashima, "Densification of sol-gel thin films by ultraviolet and vacuum ultraviolet irradiations," *Sol-gel science and technology,* vol. 8, no. 1-3, pp. 365-369, 1997.

[56] H. Podbielska, and A. Ulatowska-Jarza, "Sol-gel technology for biomedical engineering," *Technical sciences,* vol. 53, no. 3, pp. 261-271, 2005.

[57] G. Schottner, "Hybrid sol-gel-derived polymers: applications of multifunctional materials," *Chemistry of materials,* vol. 13, no. 10, pp. 3422-3435, 2001.

[58] U. Schubert, N. Huesing, and A. Lorenz, "Hybrid inorganic-organic materials by sol-gel processing of organofunctional metal alkoxides," *Chemistry of materials,*

vol. 7, no. 11, pp. 2010-2027, 1995.

[59] T. P. Chou, C. Chandrasekaran, and G. Z. Cao, "Sol-gel-derived hybrid coatings for corrosion protection," *Sol-Gel Science and Technology,* vol. 26, no. (1-3), pp. 321-327, 2003.

[60] A. Conde, A. Durán, and J. J. De Damborenea, "Polymeric sol–gel coatings as protective layers of aluminium alloys," *Progress in organic coatings,* vol. 46, no. 4, pp. 288-296, 2003.

[61] S. M. Hosseinalipour, A. Ershad-Langroudi, A. N. Hayati, and A. M. abizade-Haghighi, "Characterization of sol–gel coated 316L stainless steel for biomedical applications," *Progress in Organic Coatings,* vol. 67, no. 4, pp. 371-374, 2010.

[62] H. W. Shi, F. C. Liu, and E.H. Han, "Characterization of self-assembled nano-phase silane-based particle coating," *Transactions of nonferrous metals society of China,* vol. 20, no. 10, pp. 1928-1935, 2010.

[63] H. Wang, and R. Akid, "A room temperature cured sol–gel anticorrosion pre-treatment for Al 2024-T3 alloys," *Corrosion science,* vol. 49, no. 12, pp. 4491-4503, 2007.

[64] F. Brusciotti, D. V. Snihirova, H. Xue, M. F. Montemor, S. V. Lamaka, and M. G. Ferreira, "Hybrid epoxy–silane coatings for improved corrosion protection of Mg alloy," *Corrosion science,* vol. 67, pp. 82-90, 2013.

[65] A. L. K. Tan, A. M. Soutar, I. F. Annergren, and Y. N. Liu, "Multilayer sol–gel coatings for corrosion protection of magnesium," *Surface and coatings technology,* vol. 198, no. 1, pp. 478-482, 2005.

[66] A. F. Galio, S. V. Lamaka, M. L. Zheludkevich, L. F. P. Dick, I. L. Müller, and M. G. S. Ferreira, "Inhibitor-doped sol–gel coatings for corrosion protection of magnesium alloy AZ31," *Surface and coatings technology,* vol. 204, no. 9, pp. 1479-1486, 2010.

[67] A. Zomorodian, F. Brusciotti, A. Fernandes, M. J. Carmezim, T. Moura e Silva, J. C. S. Fernandes, and M. F. Montemor, "Anti-corrosion performance of a new silane coating for corrosion protection of AZ31 magnesium alloy in Hank's solution," *Surface and coatings technology,* vol. 206, no. 21, pp. 4368-4375, 2012.

[68] H. Shi, F. Liu, and E.H. Han, "Corrosion protection of AZ91D magnesium alloy with sol–gel coating containing 2-methyl piperidine," *Organic coatings,* vol. 66, no. 3, pp. 183-191, 2009.

[69] X. Zhong, Q. Li, J. Hu, X. Yang, F. Luo, and Y. Dai, "Effect of cerium concentration on microstructure, morphology and corrosion resistance of cerium–silica hybrid coatings on magnesium alloy AZ91D," *Progress in organic Coatings,* vol. 69, no. 1, pp. 52-56, 2010.

[70] X. Guo, M. An, P. Yang, C. Su, and Y. Zhou, "Property characterization and

formation mechanism of anticorrosion film coated on AZ31B Mg alloy by SNAP technology.," *Sol-gel science and technology,* vol. 52, no. 3, pp. 335-347, 2009.

[71] M. Garcia-Heras, A. Jimenez-Morales, B. Casal, J. C Galvan, S. Radzki, and M. A. Villegas, "Preparation and electrochemical study of cerium–silica sol–gel thin films," *Alloys and compounds,* vol. 380, no. 1, pp. 219-224, 2004.

[72] T. P. Chou, and G. Cao, "Adhesion of sol-gel-derived organic-inorganic hybrid coatings on polyester," *Sol-gel science and technology,* vol. 27, no. 1, pp. 31-41, 2003.

[73] G. C. Righini, and S. Pelli, "Sol-gel glass waveguides," *Sol-Gel Science and Technology,* vol. 8, no. 1-3, pp. 991-997, 1997.

[74] Y. Yuan, T. R. Lee, "Contact angle and wetting properties," in *Surface science techniques*, Springer Berlin Heidelberg, 2013, pp. 3-34.

[75] X. F. Wen, K. Pi. P. H. Wang, J.X. Yang, Z. Q. Cai, L. J. Zhang, and , J. Cheng, J, "Organic–inorganic hybrid superhydrophobic surfaces using methyltriethoxysilane and tetraethoxysilane sol–gel derived materials in emulsion.," *Applied Surface Science,* vol. 258, no. 3, pp. 991-998, 2011.

[76] S. Sakka, Handbook of sol-gel science and technology. 1. Sol-gel processing, vol. 3, Springer Science & Business Media, 2005.

[77] A. S. Ala'eddin, N. Ramli, and P. Poopalan, "AFM study of multilayer sol-gel Ba x Sr 1-x TiO$_3$ thin films," *Jordan Journal of Physics,* vol. 3, no. 2, pp. 61-68, 2010.

[78] V. Barranco, A. Jiménez-Morales, E. Peón, G. J. Hickman, C. C. Perry, and J. C. Galván, "Enhancing in vitro biocompatibility and corrosion protection of organic–inorganic hybrid sol–gel films with nanocrystalline hydroxyapatite," *Materials chemistry,* vol. 2, no. 24, pp. 3886-3896, 2014.

[79] M. Fedel, "Environmentally friendly hybrid coatings for corrosion protection: silane based pre-treatments and nanostructured waterborne coatings," Trento, 2009.

[80] A. Franquet, C. Le Pen, H. Terryn, and J. Vereecken, "Effect of bath concentration and curing time on the structure of non-functional thin organosilane layers on aluminium," *Electrochimica Acta,* vol. 48, no. 9, pp. 1245-1255, 2003.

[81] N. Asadi, R. Naderi, and M. Saremi, "Effect of curing conditions on the protective performance of an ecofriendly hybrid silane sol–gel coating with clay nanoparticles applied on mild steel," *Industrial & engineering chemistry research,* vol. 53, no. 26, pp. 10644-10652, 2014.

[82] L. Berzina-Cimdina, and N. Borodajenko, Research of calcium phosphates using Fourier transform infrared spectroscopy, INTECH Open Access Publisher., 2012, pp. 123-149.

[83] D. Carbonell, V. Barranco, A. Jiménez-Morales, B. Casal, and J.C. Galván,

"Preparation of sol–gel hybrid materials from γ-methacryloxypropyltrimethoxysilane and tetramethyl orthosilicate: study of the hydrolysis and condensation reactions," *Colloid and polymer science,* vol. 289, no. 17-18, pp. 1875-1883, 2011.

[84] E. Smidt, K. Böhm, and M. Schwanninger, The application of FT-IR spectroscopy in waste management, INTECH Open Access, 2011.

[85] R. F. Lenza, W. L. Vasconcelos, "Preparation of silica by sol-gel method using formamide," *Materials Research,* vol. 4, no. 3, pp. 189-194, 2001.

[86] P. J. Launer, "Infrared analysis of organosilicon compounds: spectra-structure correlations," *Silicone compounds register and review,* pp. 100-103, 1987.

[87] M. A. Karakassides, D. Gournis, and D. Petridis, "An infrared reflectance study of Si–O vibrations in thermally treated alkali-saturated montmorillonites," *Clay Minerals,* vol. 34, no. 3, pp. 429-429, 1999.

[88] M. Aizawa, Y. Nosaka, and N. Fujii, "FT-IR liquid attenuated total reflection study of TiO2-SiO2 sol-gel reaction," *Non-crystalline solids,* vol. 128, no. 1, pp. 77-85, 1991.

[89] S. Shen, D. Hu, P. Sun, X. Zhang, and A.N.Parikh, "Amino Acid Catalyzed Bulk-Phase Gelation of Organoalkoxysilanes via a Transient Co-operative Self-Assembly," *Physical chemistry B,* vol. 113, no. 41, pp. 13491-13498, 2009.

[90] B. Shokri, M. A. Firouzjah, and S. I. Hosseini, "FTIR analysis of silicon dioxide thin film deposited by metal organic-based PECVD," in *Symposium on plasma chemistry society*, Bochum, 2009.

[91] J. Méndez-Vivar, R. Mendoza-Serna, J. Gómez-Lara, and R. Gavino, "Spectroscopic study of $SiO_2 - TiO_2$ sols prepared using stabilizing agents," *Sol-Gel Science and Technology,* vol. 8, no. (1-3), pp. 235-241, 1997.

[92] D. C. L. Vasconcelos, E. H. M. Nunes, M. Gasparon, and W.L. Vasconcelos, "Infrared spectroscopy of titania sol-gel coatings on 316L stainless steel," *Materials sciences and applications,* vol. 2, no. 10, p. 1375, 2011.

[93] X. Ye, S. Cai, Y. Dou, G. Xu, K. Huang, M. Ren, and X. Wang, "Bioactive glass–ceramic coating for enhancing the in vitro corrosion resistance of biodegradable Mg alloy," *Applied surface science,* pp. 799-805, 2012.